ABSTRACT

SYNTHESIS OF SILICON OXIDE/ VYCOR COMPOSITE MEMBRANE STRUCTURES BY AN OPTIMIZED LPCVD PROCESS

by
Abhijit Datta

This study is focused on development of highly selective ceramic membrane structures consisting of silicon dioxide films synthesized by low pressure chemical vapor deposition (LPCVD) on mesoporous Vycor substrates. The ability of easily altering the composition of such films by varying the LPCVD processing parameters affords the opportunity of microengineering the pore structure by reducing the diameters of pre-existing pores in the support. The process parameters investigated include, deposition temperature, total pressure, and flow rate of oxygen. Both the kinetics and select properties of the deposits were examined. The growth rate as a function of temperature was seen to follow an Arrhenius behavior in the range 350-475 ^{0}C with an apparent activation energy of 9 kcal/mol. The growth rate was seen to increase with higher oxygen flow rate and to vary as a function of the square root of pressure. Within the framework of the process window investigated a temperature of 450 ^{0}C, total pressure of 500 mTorr, oxygen and DES flow rate of 15 sccm and 30 sccm, respectively, yielded the best quality oxide with density 2.11 g/cm^{3}, RI 1.45, and compressive stress 210 MPa. Permeation studies on Silicon Oxide/ Vycor composite membrane synthesized by the same side reaction geometry indicated poor permselectivity performance followed by cracking of the membrane structure. Opposing reactant geometry technique resulted in membrane structures of significantly higher selectivity than that predicted by Knudsen mechanism.

SYNTHESIS OF SILICON OXIDE/ VYCOR COMPOSITE MEMBRANE STRUCTURES BY AN OPTIMIZED LPCVD PROCESS

by
Abhijit Datta

A Thesis
Submitted to the Faculty of
New Jersey Institute of Technology
in Partial Fulfillment of the Requirements for the Degree of
Master of Science in Engineering Science

Interdisciplinary Program in Materials Science and Engineering

January 1995

APPROVAL PAGE

SYNTHESIS OF
SILICON OXIDE/ VYCOR COMPOSITE MEMBRANE STRUCTURES
BY AN OPTIMIZED LPCVD PROCESS

Abhijit Datta

Dr. Roland A. Levy, Thesis Advisor — Date
Professor of Physics,
Director of Materials Science and Engineering Program, NJIT

Dr. James M. Grow, Thesis Advisor — Date
Professor of Chemical Engineering, Chemistry, and
Environmental Science, NJIT

Dr. David Kristol — Date
Professor of Chemistry,
Director of Biomedical Engineering Program, NJIT

BIOGRAPHICAL SKETCH

Author: Abhijit Datta

Degree: Master of Science in Engineering Science

Date: January, 1995

Undergraduate and Graduate Education:

- Master of Science in Engineering Science,
  New Jersey Institute of Technology,
  Newark, New Jersey, January, 1995
- Master of Technology in Polymer Engineering,
  Calcutta University,
  Calcutta, India, December, 1993

Major: Materials Science and Engineering

This thesis is dedicated to
my parents

ACKNOWLEDGMENT

The author wishes to express her sincere gratitude to her advisors, Professor Roland A. Levy and James M. Grow, for their guidance, inspiration, and support throughout this research.

Special thanks to Professor David Kristol for serving as a member of the committee.

The author appreciates the timely help and suggestions from the CVD laboratory members, including: Vitaly Sigal, Dr. Lev Krasnoperov, Bozena Szkudlarski, Romiana Petrova, Venkat Paturi, Mahalingam Bhaskaran, Wei-shang King, Yan Gao, Xin Lin, Hong Wang, Dr. Jan Opyrchal and Emmanuel Ramos.

TABLE OF CONTENTS

TABLE OF CONTENTS
(Continued)

Chapter **Page**

TABLE OF CONTENTS
(Continued)

LIST OF TABLES

LIST OF FIGURES

Figure **Page**

CHAPTER 1

INTRODUCTION

1.1 Prelude

Inorganic membranes are emerging as a new class of material in recent years but their history dates back to 1940. In fact, microporous membranes fabricated from metal oxides were the first to be commercialized in a large scale gas separation process; the separation of isotopes of uranium based on differences in the molecular weight of their hexafluorides. Over the past few decades, the growth of membrane separation processes from lab-scale devices to well developed industrial unit operations have been, almost exclusively, centered around polymeric materials. The main advantage of polymers as a membrane material is the relative ease of thin film formation resulting in high permeation rates. Furthermore, new module design concepts such as liquid (1) and asymmetric hollow fibers (2) were introduced to create polymeric membrane devices with higher selectivity and better mechanical integrity.

1.2 Inorganic Membranes vs Organic Polymeric Membranes

In stark contrast to inorganic membranes, organic polymeric membrane materials are unable to fill at least two fundamental niches in separation processes i.e., high temperature (i.e., > 400 ^{0}C) gas separation and catalytic membrane reactors.

Apart from thermal stability, the motivation towards heralding inorganics as potential membrane materials is amply justified by the fact that inorganic membranes possess the following unique characteristics unmatched by their organic counterparts,

1. Structural stability and resistance to compaction, swelling, and inelastic deformation.
2. Inertness towards extremely corrosive environment and microbiological attack.
3. Ease of being regenerated by backflushing, autoclaving, and steam sterilization.
4. Flexibility to be based on a large spectrum of interesting materials unrestricted by a carbon based backbone by definition.

1.3 Potential Applications of Inorganic Membranes

Inorganic membranes have already found applications in areas such as food processing, biotechnology, pharmaceuticals, and petrochemical industry (3). Moreover, porous materials are threatening to be strong candidates for potential applications (7, 14) like separation membranes for gases, liquids and molten metals; hyper and ultra filtration for water and suspensions; separator and catalytic membrane reactor for HC conversion, and other chemical processing methods; membrane sensors for preparation of high temperature electrodes, solar cells and supercapacitors; high efficiency thermal insulators for high speed electronics as electronic and photoelectronic membranes.

1.4 Challenges and Motivation for Inorganic Membrane Research

The ever-growing vista of applications, on the other hand, poses severe demands on the membrane material scientist to engineer porous materials with high performance profiles. This in turn, requires addressing research and development issues such as,

1. Synthesizing micro/ meso porous or chemically specific adsorbent materials as required by its area of application.
2. Judiciously choosing continuous fabrication techniques for high throughput.
3. Optimizing the variables of the synthetic process in order to achieve highly permselective stress free membrane structures.
4. Implementing innovative characterization methods for assessing pore structure parameters and constructing models relating them to mechanisms of membrane transport.

A preliminary market survey conducted recently estimates that inorganic membranes could be made with permeabilities of a factor of three larger and cost per unit area a factor three times smaller than is currently available (5). The technical report strongly recommends synthesis of microporous inorganic membranes for high temperature gas separations as a promising technology

1.5 Objectives of Research

Inspired by the unique property advantages of inorganics as a separting medium, this study focused on optimizing the variables of a low pressure chemical vapor deposition process with an aim to apply these conditions to

tailor-make microporous SiO_2/Vycor composite membranes. An environmentally benign precursor, namely, DES was used for this purpose. The resulting membrane structures were characterized for perm-selectivity by a well developed in-situ technique and assessed for high temperature gas separation applications.

The main body of this thesis has been split into four additional chapters. The second chapter reviews the fundamental aspects of inorganic membrane synthesis, characterization and transport properties with a strong emphasis on the present state of art. This is followed in the third chapter by a critical review of various CVD techniques and their relevance to membrane research. Relevant properties and applicability of DES as a precursor, Vycor as a support, SiO_2 as a membrane material is also discussed. The fourth chapter is devoted to describing the experimental set-ups and procedures for synthesis and characterization techniques used in this work. Experimental data is then presented in the final chapter and analyzed at the conclusion of the thesis.

CHAPTER 2

PRESENT STATE OF ART OF INORGANIC MEMBRANE RESEARCH

2.1 Synthesis and Modification of Inorganic Membranes

The two basic types of inorganic membranes, found in literature, are non-porous and porous membranes. The International Union of Pure and Applied Chemists (IUPAC) has proposed specific nomenclature to classify porous membrane materials by their pore diameter (6).

Macroporous membrane materials have a pore diameter greater than 500Å, which is much larger than the length of mean free path of typical gases. Transport mechanisms across these porous barriers will therefore be dominated by bulk diffusion and/or viscous flow. This results in highest permeability rates and lowest selectivity during separation.

Mesoporous materials exhibit pore sizes of the same order, 20Å - 500Å, or less than the mean free path of the gaseous permeants and consequently transport mechanisms like Knudsen diffusion, surface diffusion, multilayer adsorption and even capillary transport may contribute to enhance membrane selectivity. Permeability rates maybe sensitive to specific interactions between the gas molecules and the membrane pore surface.

Microporous membranes have pore sizes less than 20Å i.e., of the same order of the permeate gas molecules. Activated transport processes, depending on molecular size, specific interactions with the porous solid, and temperature

combine to influence the extent of transmembrane flux. Much higher permselectivity is therefore possible.

2.1.1 Dense Membrane Preparation Methods

Dense membranes are nonporous and composed of metals and metal oxides belonging to Group III-V of the periodic table. They are permeable only to certain gases, such as hydrogen (palladium, platinum) and oxygen (non-porous silver, dense CaO-stabilized zirconia), exhibiting a solution diffusion transport mechanism (7, 8). The most widely studied amongst these metal membranes are composed of palladium and its alloys with ruthenium, nickel or other metals from groups VI-VIII. Palladium alloys are preferred over pure palladium since they show better resistance to fatigue and embriitlement after repeated cycles of hydrogen adsorption and desorption. These membranes exhibit infinite selectivity towards hydrogen in defect free structures. Unfortunately, thick films or thick walled tubes of palladium or platinum alloys which are commercially available exhibit poor hydrogen permeability. Paradoxically, several alloying metals of the same group show higher hydrogen permeability compared to palladium or platinum but they are highly reactive and therefore incompatible with hydrocarbon containing feed streams. Recent studies have focused more and more on obtaining metal-metal or metal-microporous ceramic composite membrane structures consisting of thinner (200Å - 2500Å) coatings of palladium or platinum (9). Base metals such as vanadium, niobium, or tantalum, microporous ceramics and glass are being typically used as support materials

due to their high hydrogen permeability, mechanical stability and relative low cost. Although, this approach led to hydrogen permeabilities 1-2 orders higher in magnitude than those for palladium membranes of the same total thickness, the durability and performance of metal-metal membranes are uncertain at temperatures above 823K (10). At high temperatures, intermetallic diffusion between the metal coating and the base metal layer reduces membrane permeability. To get around the problem of intermetallic diffusion, the use of either a barrier between the metal layers (9) or replacing metal supports with high temperature resistant microporus ceramics (11) or glass (12) is now being attempted.

2.1.2 Techniques of Porous Membrane Fabrication

Commercially available porous inorganic membranes, such as alumina, zirconia and glass, have pore diameters, 40Å to 500Å, much larger than the size of the permeating gas molecules and consequently they exhibit low separation factors. Interest in synthesizing thin microporous layers with pore sizes close to kinetic diameter of the gas molecules has therefore gained momentum in recent years.

For the first time, since the idea of molecular sieve membrane preparation was suggested (13), intensive fundamental and applied research programs are being carried out to prepare, characterize and model new generation inorganic membranes with pore sizes of 3Å - 5Å. Various approaches such as, pyrolysis, sol-gel and slip-casting, anodic oxidation, leaching, track etch, synthesis of zeolites and thin film deposition, with a common aim for a better control and

stability of pore configurations, have been proposed in literature. Several review articles, concerning this issue have been published recently (7, 14). In the following section, a brief description of each of these methods will be presented with an emphasis on identifying the process variables that control the final microstructure and the nature of disorder in the membrane material.

2.1.2.1 Controlled Pyrolysis

Organic macromolecules and certain thermosets e.g. silicone rubber (15) when subjected to controlled pyrolytic conditions, emit volatiles and finally collapse into a stable porous structure. Since, Koresh and Sofer (13), through their pioneering work demonstrated the possibility of preparing highly selective carbon microporous membranes using pyrolysis, there have been continuing efforts to synthesize molecular-sieve structures using this approach.

The key factor determining porosity of these membranes is the temperature of pyrolysis. Shelekhin et al. have showed that the final microstructure of the porous medium obtained by this technique closely approximates an interconnected network of randomly oriented inorganic fibers (18). Tomadakis and Sotirchos, therefore, argued that percolation theory could be applied on these disordered materials to ascertain morphology membrane transport properties (19). However, the future of preparing membranes by this technique depends on the formation of micro-crack free membranes at high temperatures of pyrolysis, finding preceramic precursor polymers that would finally result in membranes with high selectivity, and eliminating sealing problems associated

with membrane modules. As of now, the estimated pore diameter of molecular sieve carbon membranes prepared by pyrolizing thermoset polymers is 3Å - 5 Å showing a separation factor ranging from 4-170 depending on the combination of gases (7).

2.1.2.2 Sol-Gel Technique and Slip-Casting

Ceramic membranes fabricated by this most frequently practiced method have been commercialized and extensively reported in literature (7). Sol-gel process is multistage in nature involving preparation of a sol followed by its stabilization, gelation and finally firing at elevated temperatures to obtain either free standing or supported membrane structures.

Sol preparation requires controlled hydrolysis and condensation polymerization of metal alkoxides (i.e., Al, Ti, Zr) and/or salts to form hydrated oxide primary particles of sub-micron crystallite size. The final pore size strongly depends on the size of these precursor particles which in turn can be controlled by the nature of the solvents used, the molar ratios of alkoxides or salt to water or alcohol, the concentration and pH of the medium, temperature, stirring speed, feed rate of the reactants, and the relative rates of the hydrolysis and condensation reactions.

Once a sol is obtained, it should be stabilized in the dispersing medium to prevent aggregation of the primary particles especially during aging (14). A typical stabilization method is peptization in which mineral (i.e., HNO_3), aliphatic (i.e., acetic acid) acids, or bases (i.e., ammonium hydroxide) are added to adjust

the pH of the dispersion to increase the surface charge of the particles. It was reported that for alumina sols, the particular acid used for peptization must have an anion that does not complex with aluminum but has sufficient strength to build up the required surface charge density (20). For titania sols, it was observed that higher molar ratios of water and titania significantly affected the induction period for onset of aggregation during the aging process (21). Once a stable sol is prepared, it can either be gelled or dip coated or slip casted on a support to give composite membranes structures.

Gelation is a process of ordered aggregation that occurs when the stable sol is concentrated by solvent evaporation. Rate of evaporation that majorly affect final membrane structures in turn depends on temperature, relative humidity and concentrations of non-volatile salts.

After a stable gel structure is formed, it is fired at elevated temperatures to give the final membrane structure. The factors governing the final membrane characteristics are firing temperature, ramp time, residence time, and the incumbent environment that can either be oxidizing or reducing. Phase changes (22) and thermal and/or hydrodynamic stresses (14) that develop during the firing stage have a profound influence on the integrity of the final structure.

Sol-gel methods have been successfully employed to synthesize tiania (3, 23), silica (24), alumina (21, 25), and zirconia (3, 23) membranes. Addition of inorganic salts and dialysis that do not require solvent evaporation and thus eliminate hydrodynamic stresses during firing, are investigated as alternative gelling methods (7). Since, membranes synthesized from pure alkoxides by this

technique are generally crack free with pore dimensions between 40Å - 1000Å and of a uniform distribution, they are ideal candidates for ultrafiltration applications.

However, pore sizes less than 40Å are seldom achieved, limiting the sol-gel membranes for gas separation and catalytic applications. Future research in this area points towards formulating new strategies to fabricate microporous membranes using this method. Two recent approaches in these direction are,

Modification of sol-gel derived membranes by plugging its mesopores with materials either same or different from the parent membrane material. Al-isopropoxide in an organic solvent reduced the pore size of a gamma-alumina sol-gel membrane from 4nm to 0.5nm but permeability data suggest an unfortunate decrease in porosity during the process (25, 26).

Particle packing models suggest that for constant packing densities, the smaller the particles packed the smaller the pores formed. Based on this report, Xu and Anderson, estimated that a sol with particles less that 80Å will result in a membrane with pore sizes less than 20Å. Koreman et al. have already synthesized so called Q-particles of titania (< 30Å diameter) by carefully hydrolyzing titanium chloride. Anderson et al. are currently attempting to fabricate unsupported titania and zirconia xerogels from nano-sized particles formed by hydrolyzing titanium-tetra-isopropoxide under strongly acidic conditions for potential catalytic and photo-catalytic applications (3).

A sol with desired solid content and viscosity can be used to coat a support before it is gelled and fired. For dry porous supports, the slip-casting technique

is employed. Organic binders and/or viscosity modifiers may be added to precursor sols to enhance bonding between membrane layers and the support. The thickness of the coat depends on the contact time between the sol and the support, viscosity of the sol, wettability of the support and average size of the sol particles relative to support pore size. Good quantitative slip-casting models can be found in literature (7).

2.1.2.3 Leaching

Leaching is almost entirely devoted to the synthesis of isotropic porous glass (27) except for some porous metal membranes (14) recently being made. Leachable oxides (i.e. Na, Li, B, K) are fused together with metal oxides belonging to group IVB e.g. SiO_2 at temperatures above 1100 ^{0}C and intimately mixed. Following this, the melt extrudate is quenched at a rate rapid enough to prevent any phase separation. The resultant homogeneous amorphous material thus formed can then be subjected to a variety of time-temperature treatments. Finally, the Na_2O-B_2O_3 rich phase is water, acid, or base leached thereby creating porous structure in the SiO_2 phase. Apart from the concentration of the leachable phase, the pore characteristics can be controlled by carefully monitoring the time and temperature during thermal treatment both of which influence the spatial redistribution of the phases.

For thermal treatments at 400 ^{0}C, the rate of redistribution of soluble component is slow. and thus nucleation of second soluble phase does not occur (28). Leaching at this stage result in microporous glass with a pore size 5Å - 20Å

as recently established by adsorption data. It was also noted that the volume fraction of the leachable phase, in this case, should be between 15vol% - 60vol% (27), which was later confirmed theoretically (16, 17).

When the homogeneous amorphous material is heat treated above 400 ^{0}C or for longer times irreversible nucleation the second phase begins. If the two-phase material is leached, a mesoporous glass membrane better known as Vycor glass is formed.

Glass membranes have a moderate separation factor of 2-5 for most documented applications, except for H_2/N_2 where permeability ratios may be between 10 and 20. Recently, microporous glass membranes with very good thermal stability (i.e., 300 ^{0}C) and very high He/CH_4 selectivity (> 10,000) have been prepared and patented by the PPG industries inc (16, 17).

2.1.2.4 Anodic Oxidation

In this technique, a thin metal foil of high purity (e.g., aluminium) is anodically oxidized in an acid electrolytic medium at ambient temperatures followed by a strong acid etch (29). The final membrane structure is highly asymmetric in nature consisting of a bulk porous layer and a thin selective membrane adjacent to the metal. The distinct feature of this technique is that it renders conical pore channels perpendicular to the macroscopic surface of the substrate and thereby approaches the ideal tortuosity factor t=1 (18). The pore diameters of the thin membrane layer show a strong dependence on the nature and the strength of the electrolyte used (7). However, these membranes have a poor hydrothermal

stability and future work in this area is expected to concentrate on this aspect.

2.1.2.5 Track-Etch Method

A radioactive source is employed to bombard particles on to a material resulting in formation of tracks that are highly sensitive to strong etchants. Typical etchants such as concentrated HF are used to fabricate mica membranes with pore diameter ranging from 60Å - 1.2μm (14). Straight round pores with uniform dimensions and distribution can be obtained by carefully controlling the time of exposure to the radiation source.

2.1.2.6 Thin Film Deposition Techniques

This technology has been primarily serving the microelectronics industry through the last decade with the primary objective of producing non-porous, wear and corrosion resistant thermally stable thin films. Recently, however, it has been demonstrated that porous metals or its alloys can form thin films on porous ceramic or stainless steel supports by conventional deposition methods. Chemical Vapor Deposition techniques are recently being employed to fabricate membrane structures by depositing metal oxide films on virgin mesoporous supports, and also as a modification process for scaling down pore dimensions in membranes synthesized by other methods. A review of composite oxide membranes synthesized by CVD is presented later (see Section 3.8).

2.1.2.7 Synthesis of Zeolites

Zeolites have been prepared by reacting sodium silicates with caustic directly on the surface of porous sintered alumina followed by hydrothermal treatment (36, 37). Recently, zeolites were incorporated into polymeric supports with an aim of preparing molecular sieve membranes but the resulting materials were either thermally unstable or show low selectivity (38). Commercial zeolite based membranes show a separation factor of 3.3 for oxygen enrichment applications.

2.1.3 Structure and Configuration of Inorganic Membranes

Porous ceramic membranes can either be single-layered or composite. The composites or graded structures are a combination of at least two components i.e., a mechanically tough porous support a few mm thick and a thin selective layer with finer pores superimposed on it. This top layer, a few microns thick may be deposited either as a continuous film or in a discontinuous manner within the pore channels of the substrates. Intermediate or buffer layers between the membrane and the support have also been attempted to avoid or reduce penetration of membrane precursor particles into support pores. Any significant penetration might cause pore blockage and thus a reduced permeability through the composite membrane structures (7).

Generally speaking, inorganic membranes appear in four configurations: Flat discs or sheets, tubes, and multichannel monoliths and hollow fibers. Flat discs are limited to small scale and laboratory applications, tubes can bundled into shell-and-tube configurations to improve process economics, while

monoliths may be sometimes preferred for their high specific surface area to volume ratio. Recently, it has been possible to create hollow fiber glass membranes with interesting permeabilty characteristics (39).

2.1.4 Commercial and Developmental Inorganic Membranes

Membranes with pore diameters ranging from 30Å to 5μm are commercially available. Typical porosity between 30% to 60% by volume provides a good compromise between selectivity and permeability. Sharp pore size distributions have been achieved through control over the precursor dimensions (3) and/or post-synthesis operations to promote densification and orderly particle stacking (22).

Commercialized membranes with pore sizes between 40Å - 500Å are primarily focused on liquid phase separations. They can be conveniently categorized into four types:

1. Zirconia (Ucarsep, Carbosep, Dynaceram, etc.)
2. Alumina (Membralox, Ceraflo, Anopore, etc.)
3. Glass (Vycor, Ashai, Schott, etc.)
4. Porous metals (Monel, Stainless Steel, Hastelloy, etc.)

A comprehensive summary of these membranes can be found in literature (14). Developmental membrane research is concentrating more and more on achieving microporous pore dimensions, which are effective in high temperature gas separation or catalytic reactor based applications.

2.2 Mechanisms of Membrane Transport

As the database on permeation of different gases through a wide range of inorganic membrane materials keep on expanding, it becomes possible and necessary to develop a quantitative theory. Theoretical models relating gas diffusion and permeation in microporous molecular-sieve membranes to temperature, pressure and the kinetic diameter of the diffusant are found in literature (18). Although decrease in diffusant's diameter usually results in high transmembrane fluxes in molecular sieves, special attention needs to be focused on absorbable gases or vapors and highly tortuous diffusion paths in the membrane.

The driving force for transmembrane flux is derived either from a pressure differential between the feed side and the permeant side of the porous barrier or from a difference in concentration, partial pressures or chemical potential.

Factors like specifics of membrane preparation technique, final structure of the porous material and membrane diffusant interactions interplay to determine the contribution that each mode of transport might have on perm-selectivity data. Identifying the dominant mode of membrane transport, therefore, is an absolute necessity to boost membrane performance. A good starting point leading to such an understanding is to have a clear view of the individual modes of transport in their unperturbed state. Convective flow can be ignored for transport across meso and microporous membranes under discussion. Four separate modes of transmembrane flux will therefore be discussed.

2.2.1 Diffusion

This mode of membrane transport is based on the random-walk mechanism and on the assumption that molecules are infinitesimal points. The distribution of jump distances, therefore, is not only directionally random in nature but also the same for all molecules (40). The diffusion coefficient, irrespective of the kinetic diameter and chemical nature, is then directly proportional to the average molecular velocity of the gas molecules, and two gases can be separated by an amount equivalent to by the inverse of the square root of the ratio of their molecular weights (Equation 2.1).

$$\frac{\alpha_1}{\alpha_2} = \sqrt{\frac{M_2}{M_1}} \tag{2.1}$$

where, α_1, α_2 = permeability of permeate (1) and permeate (2); M_1, M_2 = molecular weight of permeate (1) and permeate (2).

Gas molecules that obey this relationship under certain conditions are said to exhibit Knudsen flow behavior (41). This result holds true for both multicomponent and single component systems. However, infintesimality in dimension is an idealism and the diffusion coefficients of only those molecules with mean free paths much larger than their diameter will approach classical values predicted by Knudsen. When the sizes of the molecules are of the same order as their jump distances, the mean free path is shorter by an amount that scales with the diameter of the molecules (42). Application of hard sphere model

modifies the classical Knudsen equation, in this case, by a factor that is essentially the ratio of the difference between the mean free path or capillary diameter and the molecular diameter (Equation 2.2).

$$\frac{\alpha_1}{\alpha_2} = \sqrt{\frac{M_2}{M_1}}\left(\frac{D-\sigma_1}{D-\sigma_2}\right) \tag{2.2}$$

where, D = pore diameter; σ_1, σ_2 = kinetic diameter of permeate (1) and permeate (2).

Most gaseous species have molecular weights between 10-100 and therefore it is rare to find a gas mixture for which an efficient separation by Knudsen diffusion is possible.

2.2.2 Specular Reflection

Knudsen's theory is based on the assumption that elastic collisions between the molecules and with the walls are essentially random in nature. Based on gas flow anomalies, Maxwell (41) was the first to point out that momentum, in specific cases, may not be conserved during collisions, and therefore, a fraction of the molecules may be specularly reflected from the walls. This ordered phenomena increases the effective diffusion coefficient and the flow rate especially for gases with lower molecular weights and adsorptivity (42).

2.2.3 Adsorption

Adsorption is particularly dominant at low temperatures when the interaction potential between the permeate and the porous material is significant. Adsorption of gases in the pores of a membrane material can significantly deviate permeability data obtained from pure diffusion by altering the effective pore diameter. Even, a monolayer adsorbed inside the pores decrease the effective size of the pore channels by approximately two molecular diameters. Both monolayer and multilayer adsorption, lead to other interesting modes of membrane transport (43).

2.2.3.1 Capillary Condensation

Multilayered adsorption can lead to condensation in pore capillaries when partial pressures of a particular gas is close to its vapor pressure. At steady state, the condensed gas completely blocks the pores preventing non-condensable gas molecules to transit across the membrane and thus an infinite separation factor is achieved (44). This mode of membrane transport can be used to advantage to achieve desired separation and recovery if careful considerations are given to the choice of membrane materials relative to the feed stream and membrane operating conditions. Kelvin's equation is generally used to obtain a rough estimate of the relative pressures at which condensation occurs. Some alumina membranes can effectively separate water vapor from air or alchohol by this mechanism with a separation factor of 7-460 (45).

2.2.3.2 Surface Diffusion

Surface diffusion is important when one component is preferentially adsorbed. The adsorbed molecules accumulate subsquently hop from point to point along the surface, with no apparent residence time in the bulk phase. Preferential surface adsorption and diffusion cause a difference in the permeability rates and consequently separation. Since the energy state of the diffusing species is dominated by its interaction with the surface, the surface chemistry of the membranes play a key role (46). The size of the pores are less important, although, it has been estimated that the pore dimension must be less than 10 atomic diameters before surface diffusion becomes dominant over bulk transport (39). Apart from Vycor glass, microporous alumina and hollow fiber silica membranes exihibit this mechanism of diffusion (47, 33-34). An anomalous increase in permeability for certain polar permeants (i.e., CO) across these membranes were observed recently, and attributed to enhanced surface coverage due to their interaction with the active oxide surface. Surface diffusion is generally assumed to be an activated process and additive to bulk diffusion estimates.

2.2.4 Configurational Diffusion and Molecular Sieving

Gas separation by these mechanims is often encountered in microporous thin layered inorganic membranes with pore sizes of the order of 2-3 molecular diameters of the permeates. Only certain gases with kinetic diameters less than the size of the pores can transit across the membrane. Adsorption effects are

assumed to be negligible and therefore the chemical nature of the permeants are unimportant while computing flux. Since, well defined pore sizes and sharp pore size distributions are easy to achieve in zeolites, they are ideal for separating gases based on this size-exclusion principle. However, zeolite membranes tend to exhibit strong sensitivity towards the geometry of the permeants. This led to the identification of a new mode of transport, viz., configurational diffusion (36).

Molecular sieve carbons, on the other hand, show a strong tendency to follow an element of this behaviour in their ability to interact with molecules of slight size differences at dramatically different rates. Molecular sieves derived from polymer pyrolysis (13) are highly disordered materials composed of a heterogeneous array of interconnected pores and tortuous pore channels (18). As permeating molecules pass through these constrictions they experience varying energy fields due to pore wall effects. Transmembrane flux and therefore selectivity is controlled by the largest activation energy barrier (39).

2.3 Characterization of Pore Structures

Porosity is a property of solids that is due to their structure and is characterised by the presence of voids between separate grains, layers, crystals and other elements of a coarse structure of a solid. This definition emphasizes the fact that pores are spaces not only between the molecules but between the supermolecular structures. Pore dimensions are intimately related to the modes of membrane transport. Structural informations and estimates of porosity are

therefore central to the evaluation of membrane quality and performance. Moreover, for composite membranes substrate pore configurations are key factors influencing perm-selectivity in the final composite structures. The intricate issues which concern the ongoing research in this area are,

1. Physical and chemical inheterogenities of the membrane material.
2. Influence of the probe on pore characteristics leading to changes in pore dimensions during characterization.
3. The diversity of membrane modules and pore structures which are complicated by shape and totuosity factors.

The methods of quantifying pore structure beginning with the classical to the recent innovative ones will be discussed now.

2.3.1 Gas or Vapor Sorption

Estimating pore dimensions by this classical method is based on determining the amount of vapor of a low molecular weight liquid or a gas at low temperatures, that is adsorbed by a specimen at different vapor pressures. This is usually done by measuring the increase in mass of the adsorbent with the aid of a very sensitive spiral balance or by simply determining the loss of vapor form a calibrated volume. The adsorption data can then be fitted to different isotherm models. The standard approach used is the BET modified Langmuir isotherm equation which accounts for multilayered adsorption and also shows a linear behavior when adsorbed volume (V, typically of N_2 at 77 K) is plotted against the relative pressure (p/p_0) in the range 0.05 to 0.3.

The slope of this plot gives the desired monolayer capacity (V_m) and the Y-intercept contains information about adsorbate-adsorbent interactions. The surface area can then be calculated from a knowledge of the cross sectional area of the adsorbed molecule. At high relative pressures, hysteresis is commonly observed. Kelvin's equation, which relates the relative pressure at which condensation occurs to the radius of the liquid meniscus, is then employed to give more precise pore dimensions and distributions.

A wide variety of mesoporous solids have been characterized by excellent commercially available instruments. However, since the pore size bears an exponential relationship to the relative pressure, this approach fails for pores bigger than 50nm (48)

Micropores are under conditions of interacting potential fields due to wall effects, therefore, Dubinin-Radushkevich equation (Equation 2.3) based on a theory proposed by Polyani and Dubinin can be effectively employed.

$$= W_0 \exp\left(-A\frac{e^2}{\beta^2}\right), \quad \text{and,} \quad e = RT\ln\left(\frac{p_0}{p}\right) \tag{2.3}$$

where, W_0 = limiting adsorption volume; e = adsorption potential; p, p_0 = partial pressure of the adsorbent before and after saturation; A, β = empirical constants.

The distinct advantage of this approach over BET is that adsorption isotherms plotted as ln(W) versus e^2, yield a straight line, independent of the nature of the adsorbent and the temperature. Any deviations from the linear behaviour would therefore suggest a pore size large enough to facilitate capillary condensation. Pore size estimates using this model have been attempted with success recently (16, 17).

2.3.2 Mercury Porosimetry

In this method of pore characterization the sample is evacuated and placed in a mercury atmosphere. Mercury, due to his high surface tension, does not wet most surfaces and therefore must be driven through the pores by a pressure gradient given by the Washburn equation (Equation 2.4).

$$r_p = \frac{-2\gamma * COS(\theta)}{P} \tag{2.4}$$

where, r_p = pore radius; γ = surface tension of mercury; θ = contact angle; P = pressure.

Mercury porosimetry typically estimates pore size by measuring the loss in the volume of mercury with increasing pressure differential, required to drive it through the pores. Apart from network and percolation effects , which are biased towards smaller pore sizes, this technique is also limited by uncertainties in contact angles and surface tension measurements, inability to estimate microporosity, the need to prepare dry samples, and compression with

subsequent destruction of the samples at high operating pressures. However, advantages like high volume resolution and automated, rapid analysis explains its popularity as a pore characterization technique for a wide range of meso and macroporous materials (48).

2.3.3 Permporometry

This method of characterization is relatively new and is used to examine changes in pore size distribution of porous ceramic substrates due to deposition of solid oxide within them. Pores are first blocked in a controlled manner by capillary condensation of a chosen vapor phase and gas diffusion flux is simultaneously measured through the remaining open pores (49). The condensable vapor phase should have a high vapor pressure and a high evaporation rate, and should be inert to the specimen to be characterized. CCl_4 due to its good wettability and small spherical configuration is an ideal standard vapor phase, although, cyclohexane is sometimes preferred (50). A typical measurement protocol of this method will consist of saturating the substrate by condensing the vapor in the capillary pore channels so that no gas diffusion across the barrier is possible. On subsequent reduction of the relative vapor pressure of the condensed phase, pores only with radii equal to or larger than a corresponding size determined by the Kelvin equation, will be opened and available for diffusion (Equation 2.5).

$$\frac{2Cos(\theta)}{r} = -\frac{RT}{\sigma_1 V_m}\ln\left(\frac{p}{p_0}\right) \qquad (2.5)$$

where, θ = contact angle between the liquid and the pore wall;.V_m = molar volume; r = radius of the cylindrical pores; R = gas constant; T = temperature in Kelvin; σ_1 = kinetic diameter of the diffusant.

The vapor pressure of the condensed phase can be decreased gradually and the consequent change in flux of a permeate through the membrane can be measured. Pore size distribution can then be calculated from this data (51). One advantage of permporometry is that it measures only the open pores, i.e. those which contribute to gas diffusion. However, any deposition on the substrate would incorporate errors in the results as this technique which do not account for any extra layers that may be formed during the deposition process (50).

2.3.4 Small Angle Scattering Techniques

Small angle scattering (SAS) techniques are emerging as efficient tools for structural analysis in recent times (48). Variations in scattering-length density (neutrons; SANS), electron density (x-ray; SAXS), refractive index (light; SALS) give rise to diffuse scattering characterized by an inverse relationship between pore size and the scattering angle. Intensity data are plotted against the scattering vector, Q. The scattering vector is the spatial Fourier wavelength of the fluctuations due to diffuse scattering and therefore can be related to the scattering angle. Since most porous materials are amorphous, diffraction data

obtained from large angle techniques are very difficult to interpret. In contrast to this, in the small angle and small Q regime, simple power laws equations based on fractal geometry can be effectively employed to offer simple interpretation of scattering profiles of amorphous membrane materials. Moreover, Guinier's approximation which applies at small Q can be used to give mean pore radius of gyration from which radius of pores with different shapes can be calculated and compared to estimates of pore dimensions obtained by other methods (48). Ongoing studies have shown the high sensitivity of this technique to changes in pore surface characteristics. Significant shifts in the spectrum are observed during vapor adsorption, capillary condensation and changes in surface contours. However, SAS methods which detect charge density changes, fail to differentiate between scattering pores from inclusions. Contrast-matched adsorbates may therefore be used in specific cases to obtaining pore dimension informations in two-phase materials (48).

2.3.5 Nuclear Magnetic Resonance

NMR spectroscopic technique (52) is based on the quantization of the magnetic moments of many nuclei when subjected to a magnetic field. Energy transitions typically occur in the radio-frequency range and is characterized by the peak position, chemical shifts, and two relaxation times. NMR is so sensitive to changes in local environment of the nucleus that chemical shifts, to 0.01ppm, from a reference compound can be accurately determined. The longitudinal relaxation time T_1 which determines the rate at which the magnetization returns

to equilibrium along the applied field, is shorter for molecules near the walls of a pore than those at the center. Pore Size Distribution can therefore be obtained from a distribution of relaxation times and pore radius estimated from Equation 2.6.

$$\frac{1}{T_1} = \alpha + \frac{\beta}{r_p} \tag{2.6}$$

r_p = hydraulic pore radius; α = constant related to T_1 of a pure fluid; β = constant related to T_1 of the molecules at the wall.

The transverse relaxation time is not taken into account during pore dimension calculations as interactions that influence T_2 are difficult to control and quantify. Extensive research in this area have revealed a decrease in sensitivity of the relaxation time to pore size with increasing magnetic field since T_1 for molecules at the wall and in the bulk approach each other. The intrinsic sensitivity of this technique is directly related to the field strength and therefore, it is important to optimize the magnetic field to obtain maximum resolution. Considerations such as effects of pore-wall chemistry and structure on T_1, and inclusions in the structure, may be tantamount in obtaining more accurate estimates of pore dimensions. Chemical shift measurements of pore size which have been recently reported, shows tremendous promise especially in characterizing microporosity. The magnetic field associated with the orbiting electrons counteracts, and thereby shields the nucleus from the influence the

applied magnetic field. Any changes in bonding or in the shape of the electron cloud will therefore alter the extent to which the nucleus experiences the external magnetic field resulting in shift of the detected signal. Almost all chemical shift oriented NMR studies conducted to characterize micropores employed ^{129}Xe as the probe. The 54 electron configuration of xenon and its large size allow it to interact relatively more strongly with the pore walls. In fact, it has been observed that ^{129}Xe chemical shifts are extremely sensitive to changes in density (48) and therefore to pore size of the membrane material.

The ^{129}Xe chemical shift in the pores is typically measured as a function of pressure. Extrapolation to zero pressures eliminates effects due to intermolecular collisions and thus the mean free path of the diffusant is solely dependent on the pore size, irrespective of its chemical constitution. ^{129}Xe chemical shift NMR technique has been successfully employed to characterize zeolites, but it fails for materials with pore sizes greater than 10Å (52). Several groups are pursuing this technique with an aim to find other suitable gas probes at varying temperatures to obtain reliable estimates of a wider range of pore sizes. It is worthwhile mentioning here that one unique advantage of NMR over sorption and porosimetry is that it does not require either fluid exchange or pore drying during characterization and thus possibilities of changes in pore configuration during measurement is eliminated. It has also been reported that, NMR studies also provide useful information about the hydrolysis reactions which occur during the formation of the sol particles (3).

CHAPTER 3

EVALUATION OF LOW PRESSURE CHEMICAL VAPOR DEPOSITION AS A MEMBRANE SYNTHESIS TECHNIQUE

3.1 Overview of the CVD Process

Chemical vapor deposition is essentially a material synthesis technique in which three major sequential steps are involved (53, 54):

1. Bulk diffusion and adsorption of reactants, diluents and carrier gas on to the substrate.
2. Diffusion, dissociation and chemical reaction on the surface of the substrate resulting in film formation.
3. Desorption from the substate surface, and finally evacuation of gaseous by-products of the reaction from the chamber by bulk transport.

3.2 Kinetics of the CVD Process

The formation and subsequently the quality of chemical vapor deposits is determined both by heterogeneous and homogeneous reactions, and the extent that one is favored over the other.

Heterogeneous reactions which occur on or in close vicinity of the substrate surface, are usually bimolecular in nature following the Langmuir-Hinshelwood mechanism where (54),

$$D.R. = \frac{k_2 K K' P P'}{(1 + KP + K'P')^2} \qquad (3.1)$$

where, P and K are the pressure and adsorption coefficient of one reactant; P' and K' are the pressure and adsorption coefficient of the other reactant. If the pressure P' is kept constant, and P is varied, deposition rate first increases, levels off and then decreases.

Homogeneous reactions i.e. reactions occurring in the gas phase may be unwanted because they can generate large clusters in the gas stream thus degrading film quality. Homogeneous coverage may be possible by keeping a low Sherwood number but inhomogenities in the radial thickness profile of the films can't be avoided. Sherwood number is inversely related to the diffusion coefficient of the reactant species (55).

The kinetics of film growth in a CVD process is typically governed by either a surface reaction rate or the rate at which the reactants approach and impinge on the substrate depending upon which is the slowest. Adsorption of decomposition products on the substrate surface may be an additional factor retarding rates of film growth. However, desired deposition kinetics can be achieved by a judicious adjustment of the process variables. Growth at low temperatures generally tend to be surface reaction rate limited (56).

3.3 Categories of CVD

Amongst the CVD processes the most popular and widely practiced techniques for depositing thin films are atmospheric pressure CVD (APCVD), Low pressure CVD (LPCVD), and plasma enhanced CVD (PECVD).

Thin films deposited at atmospheric pressures lack in uniformity and step coverage primarily because of the comparable rates of the heterogeneous and homogeneous reactions.

PECVD uses rf-induced glow discharge as the energy source, and allows opportunities for low pressure operations. Consequently films deposited by this low temperature technique are generally uniform with good adhesion, especially when high rf and gas flow rates are used. However, conformal step coverage of these films are not good and pinholes counts may even be high. Furthermore, nitrogen and hydrogen often get incorporated into these films and stoichiometric compositions are difficult to achieve (57).

LPCVD technique, which allow flexible temperature operations in the low pressure regime, has been used in this work and will be discussed at length in the following section.

3.4 Low Pressure CVD (LPCVD)

The pioneering work of Tanikawa et. al. in 1973 (58) established that low pressure deposition principles lead to closer packing of the substrates i.e. a higher throughput, while keeping the films uniform. At low operating temperatures the mean free path of the gas molecules increases with a

concomitant decrease in the thickness of the boundary layer. Diffusive mass transfer rates are therefore greatly enhanced over surface reaction rates lowering the possibility of gas phase reactions (54). A great variety of defect free stoichiometric films of polysilicon, silicon nitride, silicon oxide, boron nitride and tungsten with excellent uniformity and conformal step coverage have been synthesized by the horizontal tube hot wall LPCVD process (53). However, the growth rate and the quality of the films depends on the optimization of the following process variables:

1. Temperature: Surface reaction rates are very sensitive to temperature, following an Arrhenius behavior, characterized by the rate Equation 3.2. Radial heating with resistive coils is usually employed to maintain isothermal conditions between the substrate and the reactor wall throughout the process.
2. Total pressure of the process: Under conditions of constant temperature and reactant flow rates, growth rate follows an Langmuir-Hinshelwood mechanism as already discussed. At higher pressures, the residence time of the reactants increases with an accompanying increase in the probability of gas phase reactions.
3. Partial pressures and flow rates of the reactants: Deposition rates usually increase with increasing partial pressures of the reactants. Increasing deposition rates by increasing the partial pressure of the reactants in turn enhances the probability of undesired gas-phase reactions as the surface of the substrate gets saturated.

The major disadvantage of the LPCVD process however is low deposition rate and therefore poor yield (59). According to Equation 3.2, increase in temperature will result in exponential increase in the growth rate, but the resulting thermal stresses might be detrimental to the integrity of the films.

$$D.R. \propto Ae^{-\frac{E_a}{RT}} \tag{3.2}$$

where, A = frequency factor; E_a = actvation energy.

Numerous attempts using a large variety of precursors have been made to synthesize SiO_2 films at the low, medium and high temperature range. LPCVD of SiO_2 films was carried out using silane as a precursor. The films synthesized at a low temperature (310 ^{0}C-450 ^{0}C) showed high depletion, high etch rates, low R.I., and low density values. The growth rate have been reported to increase with temperature giving an activation energy of 38.5 kJ/mole (61). However, heating at 700 ^{0}C-1000 ^{0}C resulted in an increase in density. In the medium temperature range the films that were produced from Tetraethoxysilane (TEOS) were of excellent uniformity and step coverage, and the growth process follows an Arrhenius behavior in the temperature range 650 ^{0}C-800 ^{0}C with an apparent activation energy of 183 kJ/mole (60). Dicholorosilane as a precursor reacted with nitrous oxide in the high temperature regimes to give films of good uniformity and properties close to that of the thermally grown oxide (59).

LPCVD systems typically consist the following components (54):

1. Source reservoirs for the reactants, carrier gas and the diluents.
2. Gas/vapor feed modules equipped with mass flow controllers.
3. Reaction chamber which is generally a fused quartz tube.
4. Power source and temperature sensors to supply and monitor the energy required by the process.
5. Valves and vacuum pump assembly to control pressures accurately and also for continuous removal of by-products from the reaction chamber.

3.5 Diethylsilane as a Precursor

Alkysilanes($RSiH_3$) and di-alkylsilanes($R_1R_2SiH_2$) are being studied as an alternate precursor to silane in CVD processes because they are safer, more volatile and also produces films which have superior conformality, lower particulate contamination, low stress and higher crack resistance. The organohydrosilanes on the other hand, differ from each other in either the length or the bulk of the sustituent alkyl group. The following physico-chemical changes take place with the increase in the length/bulk of the alkyl radical:

1. Longer alkyl substituents tend to lower the activation energy of the LPCVD process (63) and the temperature of the cleavage of the Si-C bond, which in turn, results in higher growth rates at lower temperatures, albeit governed by more complex kinetics.

2. Volatility of organohydrosilanes decrease with increasing bulk of the alkyl group and metering flows calls for complex delivery systems with heated lines.

Table 3.1 Properties of DES

Chemical name	diethylsilane (DES)
Chemical formula	$SiH_2(C_2H_5)_2$
General Name	Organo-Hydro Silane
Molecular Weight	88.2 g/mole
Appearance	Colorless liquid
Solubility in water	Insoluble
Autoignition Temperature	218 °C
Normal Boiling point	56 °C
Flash point	-20 °C, (closed Cup)
Freezing Point	< - 76 °C (at 1 atm.)
Density	0.6843 g / cm^3 (@ 20 °C)
Vapor Density (air = 1)	> 1
Vapor pressure	207 Torr (@ 20 °C)

3.6 Silicon Dioxide as a Membrane Material

3.6.1 Stress

An ideal silica membrane, especially for separation at the sub-naoscale regime, should be absolutely free of cracks and pinholes, to show reproducible perm-selectivity, and to be effective as a separation medium. Stress in the deposits is actually a combination of intrinsic stress, which is a material property, and an additional component arising out of the mismatch between the thermal coefficients of expansion between the deposit and the substrate (62). Tensile stresses result in cracking of the films while compressive stresses may also be instrumental in generating stresses of tensile nature in the substrate. Optimization of process variables is therefore important to find conditions where the resultant stresses in the deposits will be minimized. Generally, it has been ascertained that above a certain temperature stress is released from the oxide films due to a bond rearrangement mechanism (63).

3.6.2 Water Absorption

Silicon Dioxide is hygroscopic in nature and therefore it tends to absorb moisture. Water molecules can either be physisorbed (i.e. loosely bound) or chemically bound in the form of silanol (OH-Si) groups. Baking at about 200 ^{0}C drives off the loosely bound water molecules, while a higher temperature (> 450 ^{0}C) is required to break the silanol bonds and release the bound water. Moisture in any form in SiO_2 is undesirable for membrane applications because it may influence either the surface chemistry or create uncertainties in

permeability data by altering the effective pore diameter. Moreover, evolution of water at high temperatures may result in an increase in the tensile stress in the film leading to cracking. The effect of moisture is compounded by the presence of porosity in the deposits. Loosely bound water molecules tend to diffuse through the micropores. The only way to minimize such a phenomena is to choose a high deposition temperature, and to optimize other process variables in order to achieve high densities close to that of the thermally grown oxides i.e. 2.27 g/cm^3.

3.6.3 Depletion, Conformal Step Coverage and Uniformity

Depletion results in a non-uniform rate of film growth along of the CVD reactor. For asymmetric composite membrane synthesis, depletion effects need to be kept at a minimum, since it might broaden the pore size distribution originally present in the substrate. This in turn, will make high permeability rates difficult to achieve even if selective separation of the permeants is obtained. Depletion effects must therefore be quantified and carefully examined with changes in the process variables.

Step coverage becomes particularly important while dealing with substrates with highly irregular contours. Pore channels, which are the desired deposition sites, are of tortuous i.e. of complex shapes and connectivity. The deposits should maintain quality and integrity over the side walls and the corners of the underlying topography so that voids do not appear upon subsequent film depositions. The mean free path of the molecules in the LPCVD process is large

enough to facilitate fill-up of narrow and complex pore channels with close packed deposits (54). Dopants can also play a key role in keeping densities constant over intricate topographies. An explanation offered to account for such a behavior was that, boron doped SiO_2, which is capable of flowing at lower temperatures, lead to higher surface mobility and better conformal step coverage (55, 64). One way of expressing uniformity is by the radial thickness variation given by, $(T_{max} - T_{min=})/(T_{max} + T_{min})*100$ where, T = thickness of the film at different points. Uniformity depends on Sherwood's number which has been already discussed.

3.7 Vycor Glass as a Membrane Support Material

Composite or graded membrane structures require a support material with the following characteristics:

1. Ability to maintain structural/ mechanical integrity over a range of high temperatures and pressures.
2. Large surface areas with mesopores providing high inherent permeabilities.
3. Narrow pore size distribution.
4. Pin hole, microcrack and defect free structures.
5. Ability to withstand property degradation in corrosive environments.

Porous ceramic substrates have a large surface area and are therefore ideal for catalyst carriers. Multilayer alumina supports are sometimes preferred since they allow high fluxes across them in addition to their ability to withstand high pressure differentials. Porous Vycor glass has long been used as a model

membrane system. It is now available in a wide variety of forms e.g. hollow fibers, capillary bundles, tubes and plates. The average pore diameter of borosilicate glass varies from approximately 40Å to 300Å, depending on the initial concentration of the boron rich phase. Vycor glass generally have a working temperature range up to 800 ^{0}C. Their resistance to alkaline solutions, particularly when hot is poor (65). Silica dissolution from glass membranes in aqueous solutions is known, and chemical treatment methods like addition of aluminum chloride into the feed stream or surface modification (33, 34) have been suggested for retarding the dissolution process. Vycor glass is steam sterilizable, mechanically and chemically stable under cleaning conditions, biologically inert and relatively less expensive which makes it suitable candidate as a support material. Quite recently microporous glass have been commercialized by the PPG industries and extensive research have been done on them (27, 16-18).

3.8 History of Composite Oxide Membranes Synthesized by CVD

Chemical vapor deposition techniques have been successfully employed for depositing solid oxide inside the pores of a suitable ceramic substrate reducing them to nano or sub-nano scale sizes. The ability of easily altering the composition of these deposits by varying the process parameters affords opportunities of micro-engineering the pore structure. Narrow deposition profiles are desired to achieve minimum intrapore resistance and therefore maximum efficiency (35).

Cao et.al. (50) employed a coupled CVD/EVD (Chemical Vapor Deposition/Electrochemical Vapor Deposition) technique to deposit yittria stabilized zirconia (Fluorite structure) on a variety of alumina discs (porosity 43%, mean pore diameter 0.16μm) by a counter diffusion reactant geometry. They studied the deposition profile and pore narrowing effects using permporometry. The summary of their observations is listed below :

Deposition profiles within the pores depends strongly on the process variables. In this case a transition of the deposition location from the surface to the inside of the pore channels was observed by varying the concentration or concentration ratio of the reactants. The width of the deposition increases with deposition temperature following the Arrhenius behaviour.

In the event of preferential deposition on the substrate surface it is very difficult to get pore closure unless a substantially long periods of deposition time was used. Surface deposition may in fact lead to no change in average pore diameter in the substrate.

A drastic narrowing of pore size distribution was observed early in the experiment with concomitant drop in O_2 permeability. This was attributed to large pore and/or pinhole filling effects and also to deposition on pore entrance.

Gavalas et al. (30) deposited films of amorphous SiO_2 within the pores of Vycor tubes (7mm OD, 4.8mm ID, 30.5cm length, 0.3 porosity, 40Å mean pore diameter), by using silane as a precursor. Depositions carried out under low pressure (8-22mTorr) using a same-side reactants geometry did not result in any significant deposition after 85min. Opposing-reactants geometry was then

attempted at the same temperature (450 ^{0}C) and 0.1 and 0.33atm. pressure of SiH_4 and O_2, respectively. The reaction was completed after 15min. and the film thickness estimated as 0.1μm. Measurements of H_2:N_2 flux at 450 ^{0}C varied between 2000 and 3000. Thermal annealing at 600 ^{0}C leads to the densification of the film further intensified by the presence of water vapor. Densification results in a loss of selectivity and permeability of the membrane probably due to shrinkage creating small microporus volumes permeable to Knudsen flow. Permeation of H_2 was believed to occur by an activated diffusion mechanism yielding an activation energy of 34.7 kJ/mole in good agreement with Lee et. al. (66) estimate for fused quartz.

SiO_2/ C/ Vycor composite membranes were synthesized by Megiris et al. (32) using tripropylsilane in an opposite reactants geometry at a high temperature to obtain better films with improved stability and resistance to shrinkage and densification. Deposition was carried out in a narrow front within the pore channels at atmospheric pressure and equal flow rates of 200ml/min. for both TPS/N_2 and O_2/N_2 streams. The concentration and the ratio of partial pressure of the reactants were also varied. The films were subjected to thermal treatments at 750 ^{0}C under O_2 atmosphere to burn loose carbon deposits. TEM studies revealed deposits both on the surface and within the pore channels. The top protective layer that was clearly visible was described to be rooted within the pore structure of the glass. The resulting composite membrane structures were thermally stable up to 800 ^{0}C and showed moderate selectivity but higher

permeation rates for H_2 when compared to SiO_2 membranes fabricated by silane oxidation. High partial pressure ratios resulted in enhanced selectivity.

Kitao et. al. (67) have applied CVD technique to modify silica membranes synthesized by the sol-gel method. That, CVD treatments were successful in plugging the pin holes left after the sol-gel synthesis was corroborated by the remarkable increase in permeability ratios of He/N_2 and H_2/N_2 and activation energies of He and N_2. The authors argued that since the molecular size of the precursor (silane) was large, SiO_2 deposition can be expected to take place preferentially within the larger pores or the pinholes. However, drop in permeability values were observed and was attributed to undesirable reduction of pores which were already perm-selective to H_2 and He. Increase in activation energy over those in parent sol-gel structures seems to confirm this argument. It is worth mentioning that activation energy values obtained for helium (8.1 kJ/mole) and hydrogen (12.2 kJ/mole) were much lower than the values calculated by Gavalas et.al.

Tsapatis et. al. (68) deposited SiO_2 from $SiCl_4$ and H_2O on porous Vycor support using standard i.e. one-sided and opposing reactants geometry and operating at atmospheric pressures at both sides of the tube. $SiCl_4$ precursors were preferred over silane to eliminate densification problems in the resultant films. Pore plugging occurred at a faster rate when reactants were metered in from the same side of the substrate. This has been rationalized as due to higher reactant concentration at the substrate surface or the pore entrances than within the pore channels. However, selectivity values for H_2/N_2 was higher (5000) for

opposing reactant geometry deposition than for same-sided (1000) one. Permeation of H_2 and N_2 at different temperatures showed an apparent activation energy of 37 kJ/mole and 60 kJ/mole respectively. However, one disadvantage of using chloride as a precursor is its corrosive nature especially in the presence of humidity.

As a conclusion, it can be said that the extensive technology of thin film deposition can be exploited to deposit selective layers on thick porous supports. Among the liquid phase deposition techniques, the sol-gel technique in combination with dip-coating has been widely used to deposit thin films on glass substrates. This deposition technique may not work well with porous substrates because of the difficulty of controlling the imbibition of the precursor alkoxide solution within the pores. Gas phase techniques such as CVD have many advantages including there ability to produce films of controllable and uniform thickness on porous substrates. Film deposition within the pore channels prevents the formation of large pinholes, protects the deposited film from loss of adhesion or other mechanical damage and affords opportunities for high perm-selective performance of the resultant membrane structures.

CHAPTER 4

EXPERIMENTAL PROCEDURES

4.1 Set-up of the LPCVD Apparatus

The LPCVD reactor schematically shown in Figure 4.1 was used to deposit silicon oxide films on silicon wafers. The reaction chamber consisted of a fused quartz reactor tube, having an inner diameter of 19.3 cm and a length of 155 cm mounted horizontally within a five zone Lindberg furnace. The furnace was equipped with resistance heating coils and capable of operating at a maximum temperature of 1200 $^{\circ}$C. Both ends of the quartz chamber were sealed with Viton O-ring caps fitted within stainless steel flanges. A type K (nickel-aluminium vs nickel-chromium) thermocouple was used to measure temperature. The precursor delivery system consisted of a temperature controlled DES (liquid) source bottle. A carrier gas for DES was not required since it has a high vapor pressure (200 Torr @ 25 ^{0}C). Reactants were metered by means of Applied Materials model AFC 550 automatic N_2 mass flow controllers which were calibrated to regulate DES and O_2 flows. All delivery lines were stainless steel with VCR type connections. The total pressure in the reactor was regulated by a feedback controlled throttle valve and monitored by a MKS Baratron pressure gauge. The apparatus was equipped with a pump assembly comprising of an Edwards high vacuum pump model E2M 80, supported by an Edwards mechanical booster pump model EH 500. An Oil filter system was

employed to prevent contamination of the pump oil thereby assuring constant pumping rates over long periods of time.

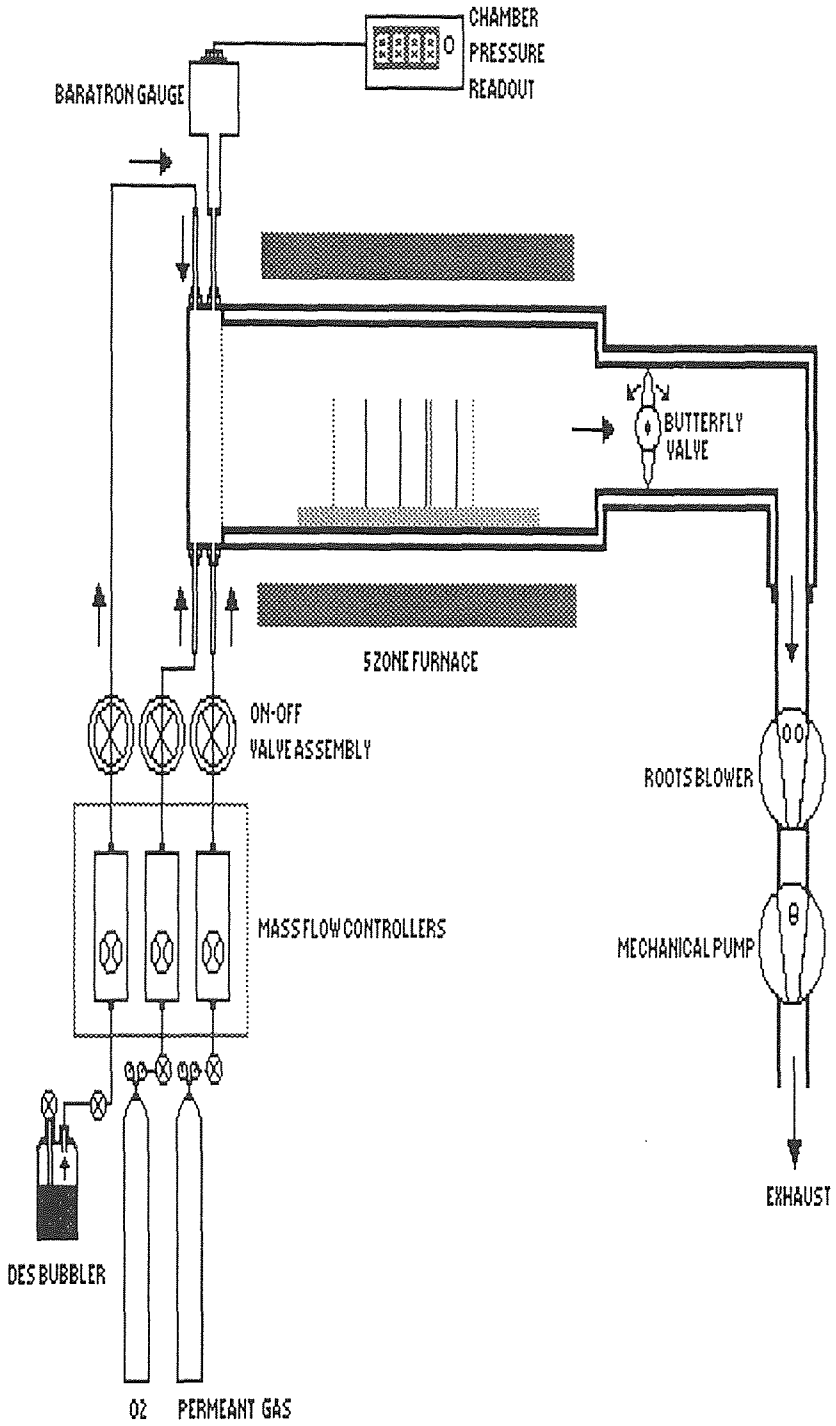

Figure 4.1 Schematic Diagram of the LPCVD Reactor

4.2 Pre-Deposition Procedure

4.2.1 Leak Check

Routine leak checks were conducted keeping all valves and mass flow controllers fully open. After evacuating the chamber, the gate valve was closed and from the pressure rise in the reactor the leak rate was calculated. Typical leak rates were of the order of 4 mTorr/min. All depositions were performed with a flat zone temperature profile and under conditions of thermal equilibrium.

4.2.2 Flow Rate Calibration

N_2 was metered into the CVD reaction chamber at a known initial pressure and at room temperature. The gate valve was then closed and the rise in chamber pressure over a fixed time interval was measured. Assuming that the temperature inside the reaction chamber temperature is at T_r (i.e., room temperature) and N_2 to be an ideal gas under these conditions, Ideal Gas Law gives,

$$PV = nRT \tag{4.1}$$

Since chamber volume, V, is fixed,

$$\frac{P}{n} = \frac{R * T_r}{V} = const \tag{4.2}$$

$$\frac{\partial n}{\partial t} = \frac{V}{R * T_r} * \frac{\partial P}{\partial t} \tag{4.3}$$

where, t = time.

At standard condition of temperature (273 K) and pressure (760 Torr) therefore,

$$V_s = \frac{nRT}{P} = nR * \frac{273}{760} \tag{4.4}$$

and,

$$\frac{\partial V_s}{\partial t} = R * \frac{273}{760} * \frac{\partial n}{\partial t} \tag{4.5}$$

Substituting equation (4.3) into (4.5), gives flow rate at room temperature of T_r,

$$F.R. = \frac{\partial V_s}{\partial t} = \frac{V}{760} * \frac{273}{T_r} * \frac{\partial P}{\partial t} \tag{4.6}$$

or,

$$\frac{760}{V} = \frac{\Delta P / \Delta t}{F.R.} * \frac{273}{T_r} \tag{4.7}$$

Where, V is the volume of the reaction chamber = 45.3, T_r is the room temperature and $\Delta P/\Delta t$ is the rate of increase in pressure. Equation 4.7 was used to calibrate the flow rate of the reactants. Special mass flow controllers for DES was not commercially available, and therefore a correction of N_2 mass flow controller which was employed to meter DES vapor, was necessary. The flow

conversion factor was obtained by taking the ratio of the flow rate of oxygen and nitrogen as shown in Figure 4.2. A similar procedure was employed to obtain the correlation factor for DES flow relative to nitrogen as shown in Figure 4.3.

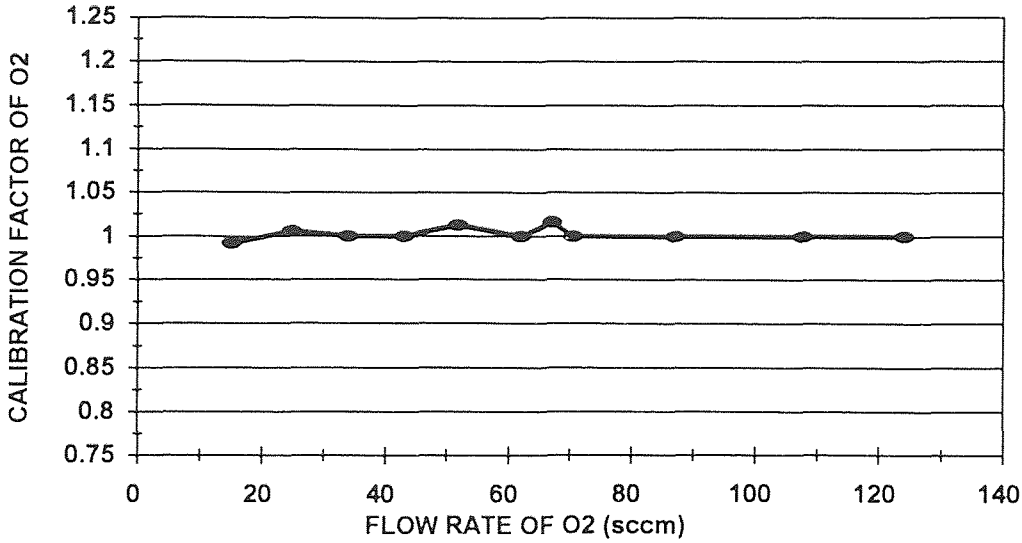

Figure 4.2 Correlation of Oxygen Flowrate to Nitrogen

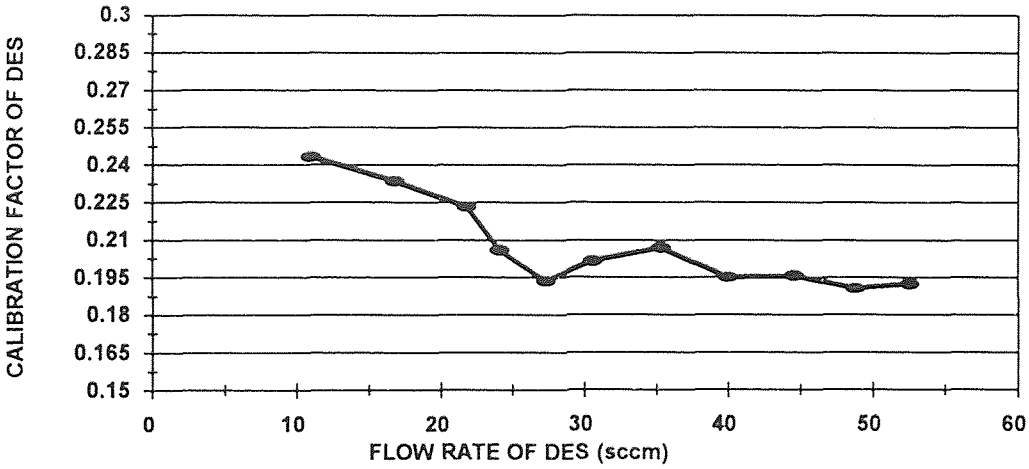

Figure 4.3 Correlation of DES Flowrate to Nitrogen

Calibration curves of the oxygen and DES flow in sccm (standard cubic centimeters per minute) against the corresponding controller set points, shown in Figure 4.4 and Figure 4.5, respectively, were employed to obtain the actual flow rates of the reactants from the set points.

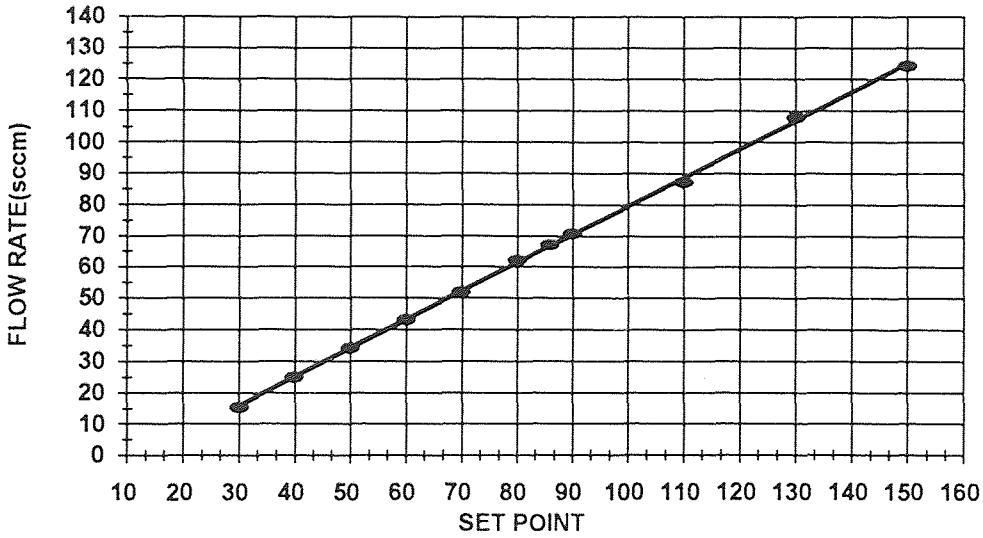

Figure 4.4 Oxygen Flowrate Calibration Curve

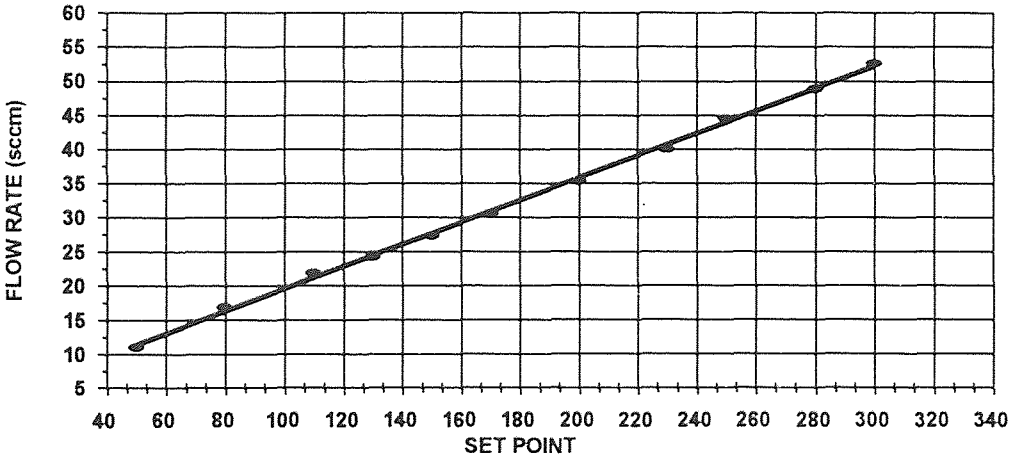

Figure 4.5 DES Flowrate Calibration Curve

4.3 Procedure for Depositing Silicon Oxide on Silicon Wafers

4.3.1 Wafer Loading

Boron doped single crystal <100> silicon wafers, polished on one side, and 10 cm in diameter, were mounted vertically on a fused silica boat with 12 single wafer slots and 10 double wafer slots. Single and double wafer slots alternated along the length of the boat with a distance of 1.25 cm between them. Four virgin and three dummy wafers were placed at the same position in each run, as shown in Figure 4.1. The first dummy wafer was mounted on the second single wafer slot at 6 cm from the front end of the boat. The first virgin wafer was then positioned on the fourth single wafer slot, 5 cm behind the dummy. The second virgin wafer was placed behind the first on the sixth single wafer slot (5 cm behind the first virgin wafer). The third virgin (<111> Si) wafer and the second dummy wafer were loaded next, back to back in the sixth double wafer slot, and the virgin wafer was dedicated to stress measurements. Behind the <111> Si wafer, the fourth virgin wafer was positioned on the ninth single wafer slot at a distance of 3.8 cm from the stress measurement wafers. The last dummy wafer was loaded on the tenth single wafer slot 2.5 cm behind the fourth virgin wafer. The distance of separation between the first and terminal virgin wafer was chosen to be 12.5 cm, closely approximating the active membrane length of the Vycor substrate. The fused quartz boat was placed with its front at 65 cm downstream in each experiment and all wafers were weighed accurately to 0.1 mg using a Mettler balance before and after deposition.

4.3.2 Setting Deposition Conditions

After the wafers were weighed and loaded sequentially on the boat. The front of the boat was placed at a distance 65 cm from the door of the reactor. The reaction chamber and the reactant delivery lines were evacuated for about 30 minutes. The reaction chamber was then gradually heated to the deposition temperature and stabilized for thirty minutes to ensure thermal equilibrium. Air blowers were used to cool the O-rings and plastic parts of the chamber. Meanwhile, DES and oxygen mass flow controllers were set to obtain the desired flow rates.

4.3.3 Film Deposition

Oxygen and DES were delivered to the reactor via separate systems to avoid the possibility of any reaction occuring in the lines. Oxygen was first introduced into the reaction chamber. As soon as a steady flow rate of oxygen was achieved (generally 2 min), DES flow was turned on. The total pressure of the reaction chamber was then adjusted and maintained at the desired value by means of a feedback controlled throttle valve. Following deposition, the furnace was cooled before downloading the wafers from the chamber.

4.4 Film Characterization Techniques

Deposition rates were determined as oxide thickness (Å) over a deposition time (min) and then averaged over four virgin wafers used for each experiment. Film

density was estimated from the fundamental mass volume relationship. Film thickness (in Å) was plotted against the half of total mass (in mg) deposited on both sides of the wafer. It was assumed that equal deposition occured on both sides of the wafer substrate, and therefore, half-mass could be taken as the mass deposited on the polished side of the silicon wafer. Since the area of the wafer is constant, density can be estimated from the slope of such a plot, if linear.

Film thickness was measured by Nanospec Interferometer which bases its estimates on the monochromatic light interface fringes formed within a zone limited by the sample surface and a semi-transparent mirror. The thickness of the film deposited on one side was measured at five different points on the wafer i.e. 1 cm off both edges of both the equatorial and the longitudinal axis, and at the center, see Figure 4.6. Uniformity in radial distribution of the deposits was then estimated from the relationship: $(T_{max} - T_{min})/(T_{max} + T_{min})*100$ where, T= the average film thickness.

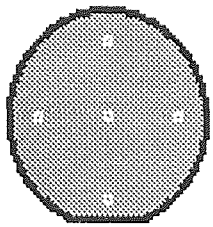

Figure 4.6 Schematic Diagram of a Typical Silicon Wafer Showing Points Where Thickness was Measured

The index of refraction values were obtained by a Rudolph Research/AutoEL ellipsometer which consists of a polarizer and a compensator. Plane (45^0) polarized light from the polarizer is elliptically polarized when it passes through the compensator. It is then reflected by the sample surface, collected by a detector, analyzed for its intensity and finally quantified by a set of delta and psi values. The values of delta and psi thus obtained, were then fed to a computer which numerically solves the equations to give the refractive index of the film.

Infrared spectroscopic analysis was done on a routine basis using a Perkin Elmer 1600 series FTIR spectrophotometer to determine the bonding characteristics of the deposits. An optical microscope, Reichert Wein (BTL 122815), was used to detect cracks, gas phase nucleation clusters, and other defects in the films.

Stress was determined by employing a device developed in-house. The device measures any change in the radius of curvature of a wafer substrate resulting from film growth on one side. Two fixed and parallel He-Ne lasers beams are incident on the wafer surface before and after deposition. The reflected beam in each case was then projected by an angled plane mirror as two points onto a scale where their separation could be more accurately measured. The change in the separation distance was then fed into Stony's equation to obtain actual stress values.

4.5 Procedure for Silicon Oxide/ Vycor Membrane Synthesis

4.5.1 Sintering of Vycor Tube

Borosilicate glass (Corning Vycor # 7930) of composition 96% SiO_2 and 3% B_2O_3 was used for this study. The Vycor substrate was of a tubular configuration open at both ends of OD 0.81 cm, ID 0.57 cm, porosity 0.28, and a continuous pore structure of average diameter 40 Å. Preceding deposition, the porous Vycor substrate was subjected, at both ends, to a well controlled sintering treatment at 1200 ^{0}C. This time-temperature treatment generated three distinct segments on the Vycor tube: a blind end, an open non-porous section and an unaffected porous part in between. The non-porous segment facilitated a leak-proof fit to the LPCVD reactor and the reactant delivery lines. The unaffected porous part comprised the active membrane area of the Vycor support, the length of which was typically between 15-20 cm.

4.5.2 Pre-Synthesis Procedure

The length of the Vycor substrate was measure before it was introduced into the LPCVD reactor through an orifice in the front door. The Vycor support was held concentric to the cylindrical quartz chamber by a series of cajon connectors fitted on to the non-porous end of the tube projecting out of through the chamber door orifice as shown in Figure 4.7. The open end of this non-porous segment was connected to gas delivery lines and a rotary-vane/ booster pump assembly via valves. Flexible stainless steel tubings were used for these connections to eliminate any possibility of stress generation during loading and dismantling

operations. A MKS baratron pressure gauge was employed to monitor changes in pressure inside the Vycor tube.

For the opposing geometry deposition procedure, a long narrow stainless steel tube was inserted inside the Vycor tube, upto 2 cm from the closed end, to enable the flow of oxygen. The feed end was connected to the oxygen delivery line and the pump assembly in a similar fashion using cajon connectors and flexible stainless steel tubings as shown in Figure 4.7.

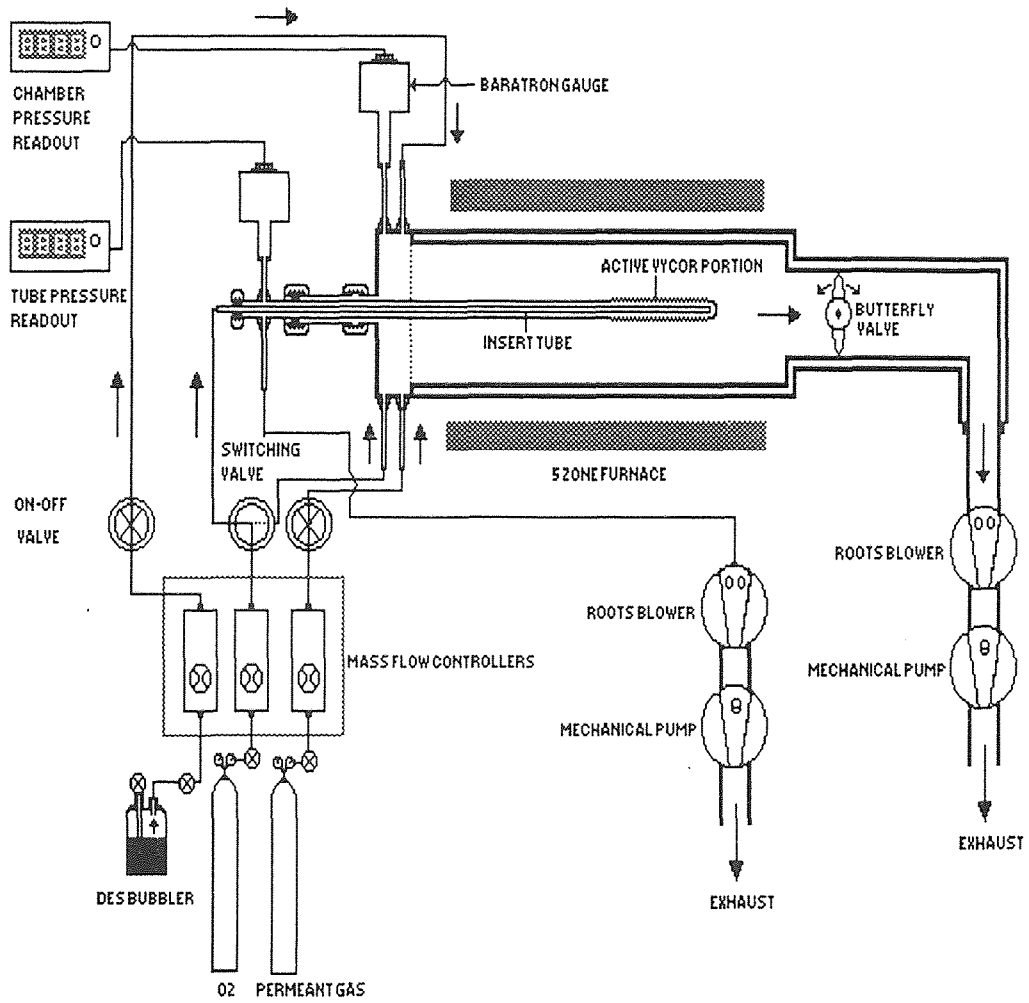

Figure 4.7 Schematic Diagram of the LPCVD Set-up for Membrane Synthesis and In-situ Permeability Measurements

4.5.3 Membrane Synthesis Method

The Vycor tube was inserted into the LPCVD reactor and evacuated. Meanwhile, the temperature was raised slowly along a ramp of 60 ^{0}C/hr and then held constant periodically after every hour, for 15 min, to ensure thermal equilibration. The LPCVD set-up was pumped down overnight to eliminate any moisture adsorbed in the Vycor and to minimize outgassing from the chamber walls. Only after an acceptable leak/outgassing rate (4 mTorr/min) was obtained, reactant flows were set and SiO_2 deposited on the Vycor substrate using the same procedure as already described in section 4.3.3. In the same side reactants geometry procedure, DES and oxygen were delivered from the chamber side with the vycor and the chamber being continuously pumped throughout the deposition process.

In the opposing reactant geometry technique the LPCVD reactor was evacuated and sealed by closing the chamber gate valve. DES was then fed into the chamber and after a desired pressure level was achieved, DES flow was switched off. Oxygen was then metered and continuously flown into the Vycor tube. Oxygen flow was set until a steady pressure inside the Vycor was obtained. After each period of deposition the oxygen delivery was stopped. The gate valve was then opened and the chamber pumped down to vacuum, before testing for perm-selectivity.

4.6 Membrane Characterization Technique

The composite SiO_2/Vycor membrane was characterized for permeability and selectivity by an in-situ technique, facilitating a rapid evaluation of membrane

performance, in between specific periods of deposition. Following deposition, both the reaction chamber and the Vycor tube were continuously pumped down until an acceptable leak rate (4 - 5 mTorr/min) was obtained. After evacuating the chamber, the gate valve was closed and appropriate pressure differentials were established by introducing a given permeate in the chamber. This pressure differential between the chamber and the Vycor tube side, provided the driving force for flux across the membrane. Gas flux across the membrane was estimated by monitoring the the pressure rise in the Vycor at specific time intervals. The rate of pressure rise, dP/dt (Torr/min), was then plotted against the appropriate pressure differential across the membrane Del P (Torr), as shown in Figure.4.8.

From the slope of such a plot, the permeability coefficient (min^{-1}) for the specific permeate was estimated. Selectivity was assessed by calculating the ratio of the permeability coefficients. The permeates were delivered under same conditions of temperature and using the same feed lines as shown in Figure 4.8.

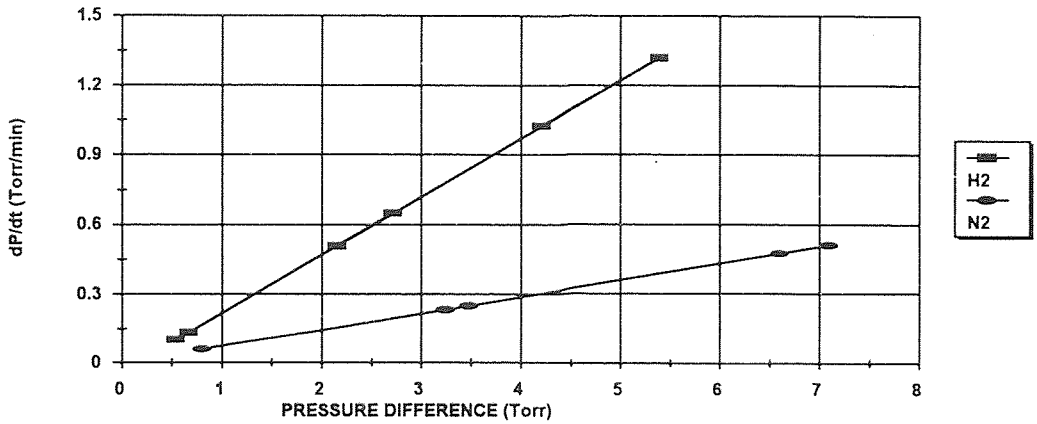

Figure 4.8 Method of Estimating Permeability Coefficient

CHAPTER 5

RESULTS AND DISCUSSION

5.1 Temperature Series

The deposition rate was studied over a series of temperatures ranging from 375 ^{0}C to 500 ^{0}C, taken at intervals of 25 ^{0}C. DES and O_2 flowmeters were set to achieve a constant flow rate of 30 sccm and 15 sccm, respectively. Total pressure inside the chamber was maintained at a constant level of 500 ±2 mTorr throughout the temperature series study.

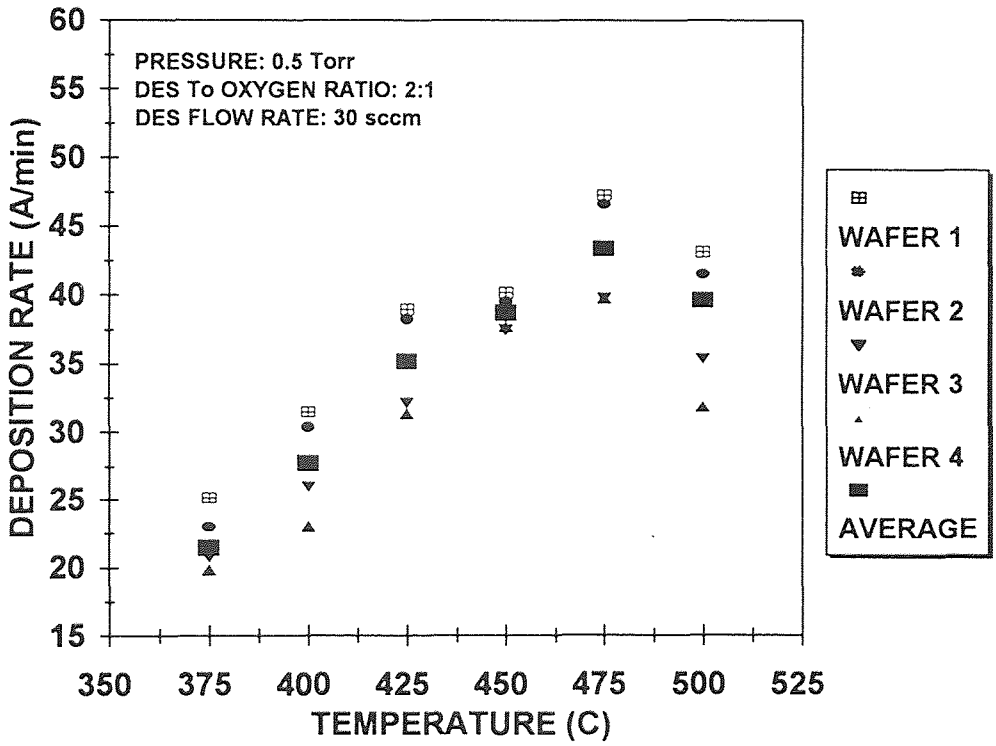

Figure 5.1 Variation of Deposition Rate with Temperature

It can be seen from Figure 5.1, that the growth rate (Å/min) increases from 21.5 Å/min to 43.4 Å/min over an temperature interval of 125 ^{0}C. However, a sharp drop in the growth rate above 475 ^{0}C indicates a transition to the mass transfer limited regime and the onset of homogeneous gas phase reactions. Increasing number of homogeneous reactions decreased the amount of the reactants reaching the wafer surface (53), which is corroborated further, in our study, by the abnormal decrease in density observed for the deposits at 500 ^{0}C as seen in Figure 5.4. Particulate cluster formation at 500 ^{0}C was also visible under the optical microscope. The formation of SiO_2 particles in the gas phase was also observed previously during SiH_4, and Triethoxysilane deposition processes (69).

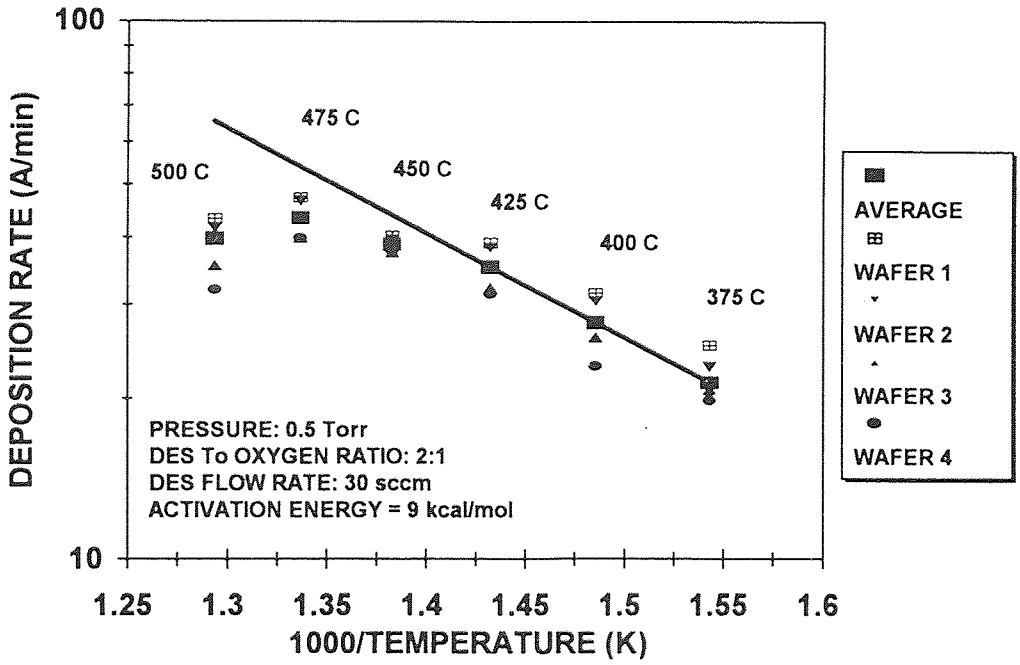

Figure 5.2 Arrhenius Dependence of Deposition Rate on Temperature

Growth rates (Å/min) plotted against 1000/T on a semi-log scale, (see Figure. 5.2) exhibited an excellent fit to an Arrhenius type behavior in the temperature range of 375 to 475 $^{\circ}$C. Film growth kinetics, in this temperature range, can therefore be assumed to follow a thermally activated heterogeneous mechanism characterized by the Arrhenius rate equation (Equation 3.2). The slope of the curve in Figure. 5.2 yielded an activation energy of 9 kcal/mol. However, activation energy energy estimates within the surface reaction rate limited regime are only apparent since they incorporate the heats of adsorption of the reactants. Furthermore, low apparent activation energy of film growth estimated from our study, is analogous to values obtained for surface adsorption mechanisms (70). Moreover, it had been observed that spacing between wafers exercise a profound influence on the resistance to diffusion of the reactants, and therefore, flow patterns and growth rates (69). Large wafer spacing used in our experiments may have played a role in determining the characteristic of the growth process.

A plot representing average film thickness as a function of half of the mass deposited on the wafers is shown in Figure 5 3. Minimal deviation from the linear least square fit indicates that, film density is not strongly dependent of temperature, in the range 375 ^{0}C - 475 ^{0}C. Knowing, that the area of the wafer is 78.5 cm^{2}, density calculated from the slope of Figure 5.3 was 2.14 g/cm^{3}. This density value is low compared to that of the thermally grown oxide (2.27 g/cm^{3}) and may be attributed either to the composition of the films or to presence of pin holes in the amorphous deposits which would tend to absorb moisture.

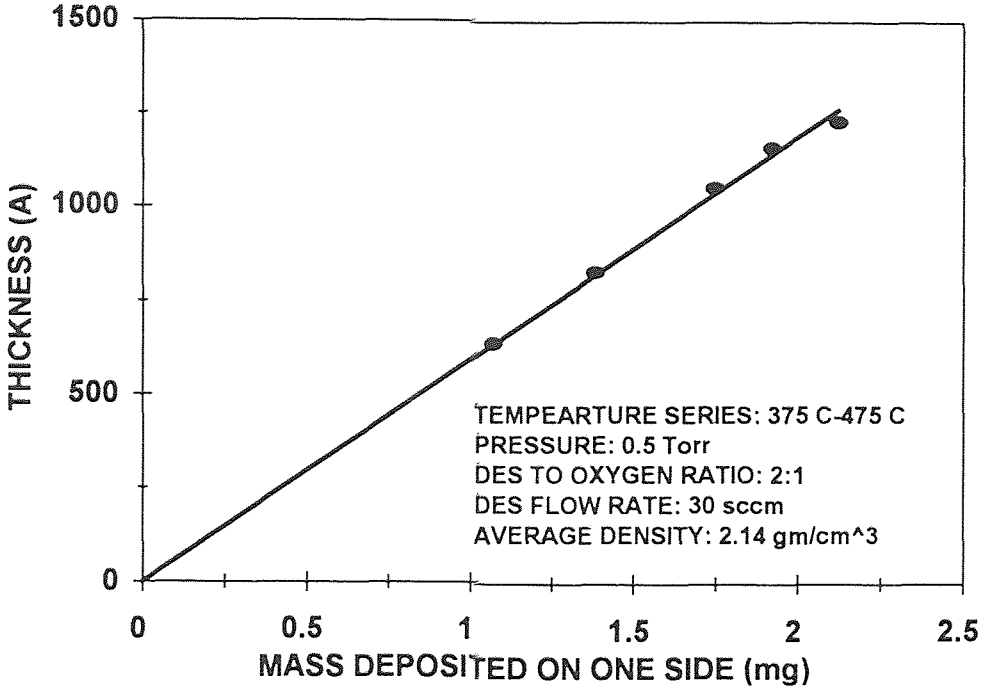

Figure 5.3 Variation of Average Film Thickness with Half of Mass Deposited on the Wafers for the Temperature Series

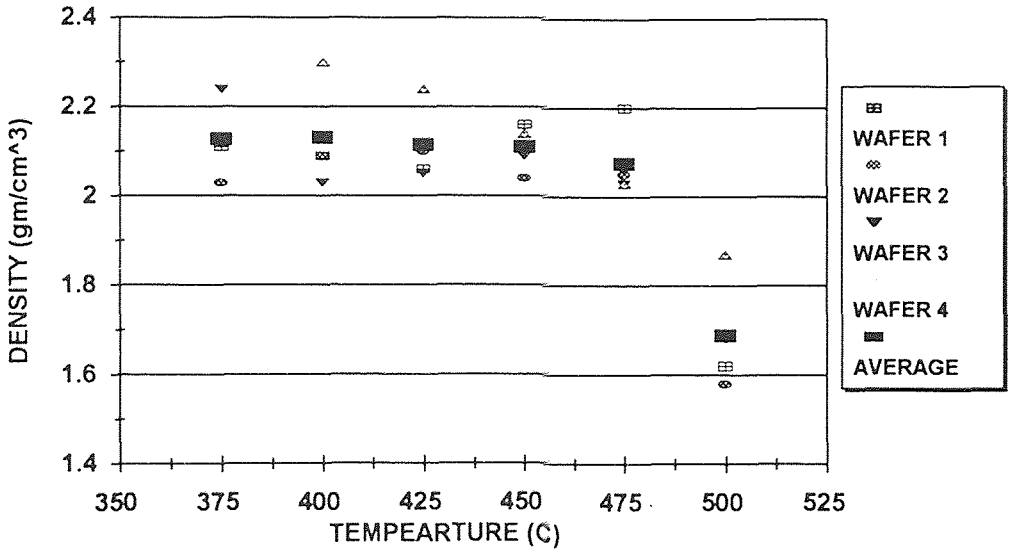

Figure 5.4 Variation of Density of the SiO_2 Deposits with Temperature

However, studying changes in the individual film density values with temperature would serve our purpose of choosing a specific thermal condition, which would yield dense deposits for subsequent membrane synthesis. In such a plot (Figure 5.4), little variation in density with temperature is observed over the range of 375-475 ^{0}C.

Depletion effects or the axial distribution of the deposits were accounted for by plotting t(0)/t(i) against the downstream distance taking the position of the first virgin wafer as the origin. t(i) is defined as the average film thickness on the i^{th} wafer and t(0) is the average film thickness of the first virgin wafer. Depletion effects shown in Figure 5.5 suggest significant deviations from ideal behavior (i.e. t(0)/t(i) = 1) which diminished steadily with increasing temperature. However, depletion was significantly lower at 450 ^{0}C than both 475 and 500 ^{0}C, possibly because increasing number of gas phase reactions at higher temperatures consume the reactants before they reach the surface of the downstream wafers.

The stress in the wafers is compressive at all temperatures decreasing with increased deposition temperature as shown in Figure 5.6. Index of refraction values evaluated using ellipsometry at a wavelength 6328 Å were 1.449 ± 0.002, a value which is lower than that for a thermal oxide (1.462) but in good agreement with the work done by Patterson et al. (69). This behavior also seemed to conform with the low density of their deposits.

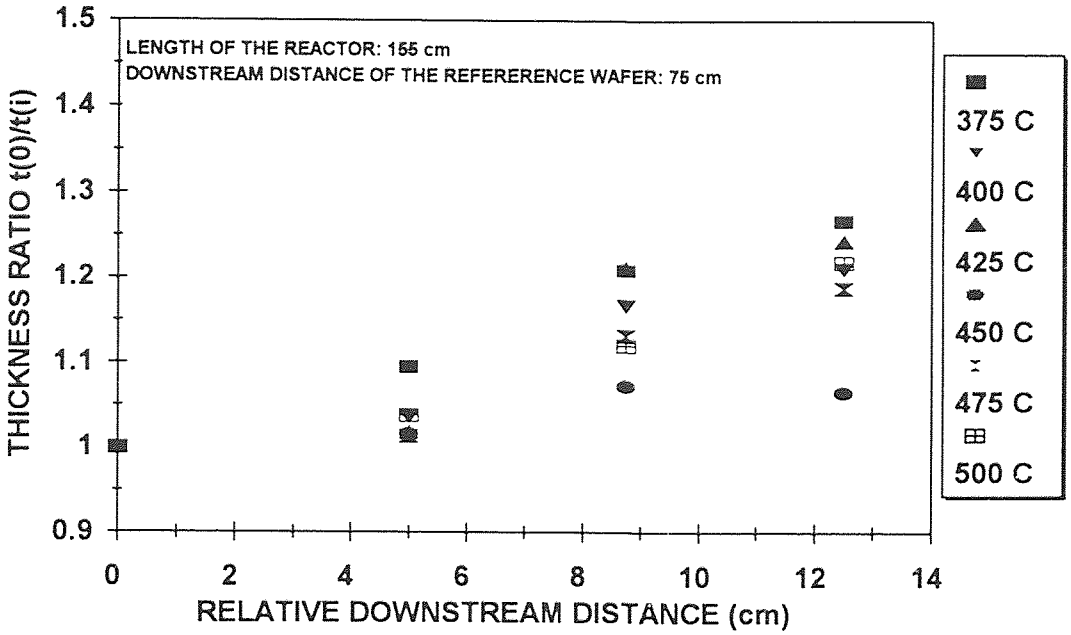

Figure 5.5 Depletion Effects as a Function of Temperature

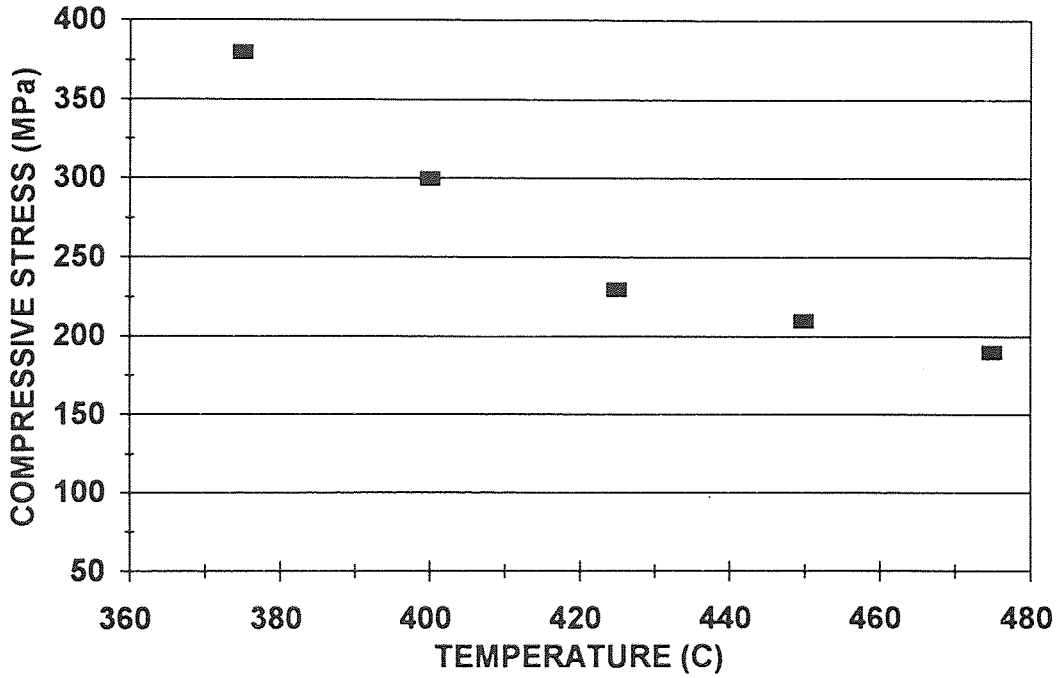

Figure 5.6 Variation of Stress in the Films with Temperature

Within the framework of the temperature window investigated, 450 ^{0}C appeared to be a plausible temperature that would yield quality oxide deposits at a moderate growth rate (38.7 Å/min). Further studies, were therefore carried out keeping the temperature invariant at 450 ^{0}C.

5.2 Pressure Series

The pressure dependent behavior of deposition rate was evaluated between 100 mTorr - 500 mTorr, at 450 ^{0}C, while keeping the flow rate constant at 15 sccm for oxygen and 30 sccm of DES.

Within the pressure window of 100-500 mTorr investigated, the growth rate was found to increase monotonically as shown in Figure 5.7. This behavior could be attributed to more and more reactants adsorbed on the wafer surface as the pressure increased. With the occupancy of an increasing number of reaction sites on the wafer surface, the probability of reaction on the surface of the substrate is enhanced and hence a higher deposition rate.

It was observed that at 50 mTorr, growth rate was so small that measurable oxide thickness could not be achieved after a 30 min deposition. Moreover, around a total pressure of 500 mTorr the deposition rate seemed to plateau. Previous work have indicated such a leveling effect at high pressures (70). Decreased rates of deposition at relatively higher pressures may therefore be due to the onset of saturation of the substrate surface by the reactants.

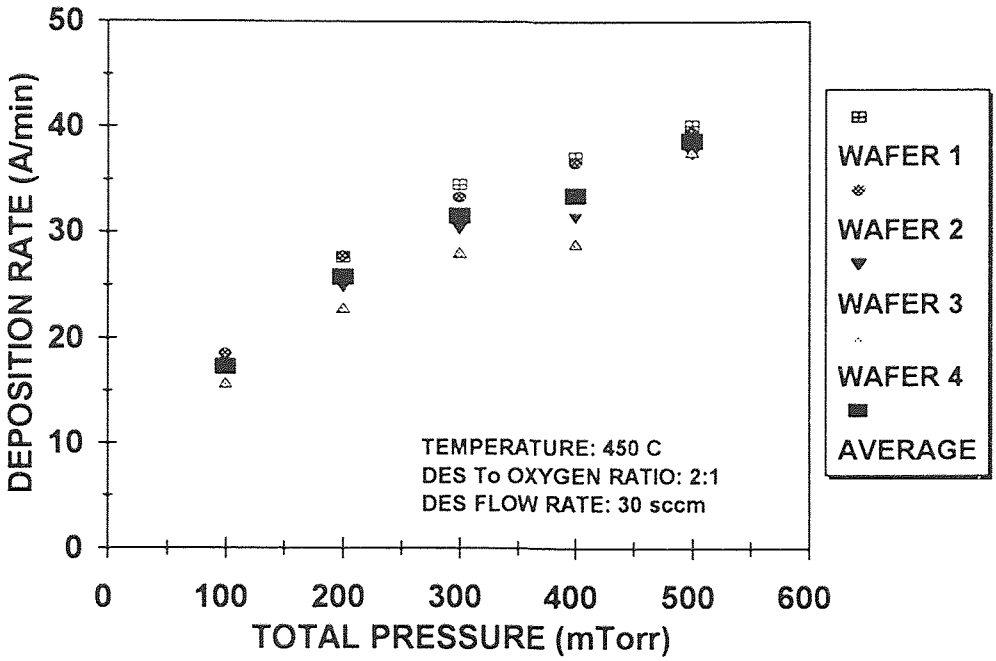

Figure 5.7 Variation of Deposition Rate with Total Pressure

Furthermore, Langmuir-Hinshelwood mechanism predicts that reaction rates within the surface reaction rate limited regime are governed by the rates of adsorption on the substrate surface as discussed in Section 3.2 of the thesis. When the interaction between the adsorbent and the adsorbate are not equal for each adsorption site and/or for intermediate pressures the Langmuir isotherm equation is reduced to $N=kP^{1/n}$ (Freundlinch isotherm, 71), where N = the number of molecules adsorbed on a surface, P = total pressure and $n \geq 1$. Growth rate, which is proportional to the number of adsorbed molecules, was found to exhibit a good least square fit when plotted against the square root of pressure in our study, in Figure 5.8, thus yielding a value of n equal to 2. A linear dependence (n = 1) of deposition rate on pressure was observed in an

earlier work in the range 550-900 mTorr, using a higher flow rate of 100 sccm DES and 200 sccm O_2 (69). Another possible explanation for the square root pressure dependence could be due to the homolytic fission and subsequent adsorption of oxygen radicals on the silicon wafer surface ($O_2 \Leftrightarrow 2O^{\cdot}$).

It was found from Figure 5.9 that density values decreased as the chamber pressure was reduced from 500 mTorr to 100 mTorr probably due to low adsorption at the wafer surface at lower pressures. It is therefore recommended not to deposit at pressure lower than 500 mTorr for subsequent membrane synthesis as undesired micro-porosity and pin holes in the pore plugs can be predicted. As already discussed, these surfaces would then be the sites for moisture absorption, thus hampering membrane efficiency.

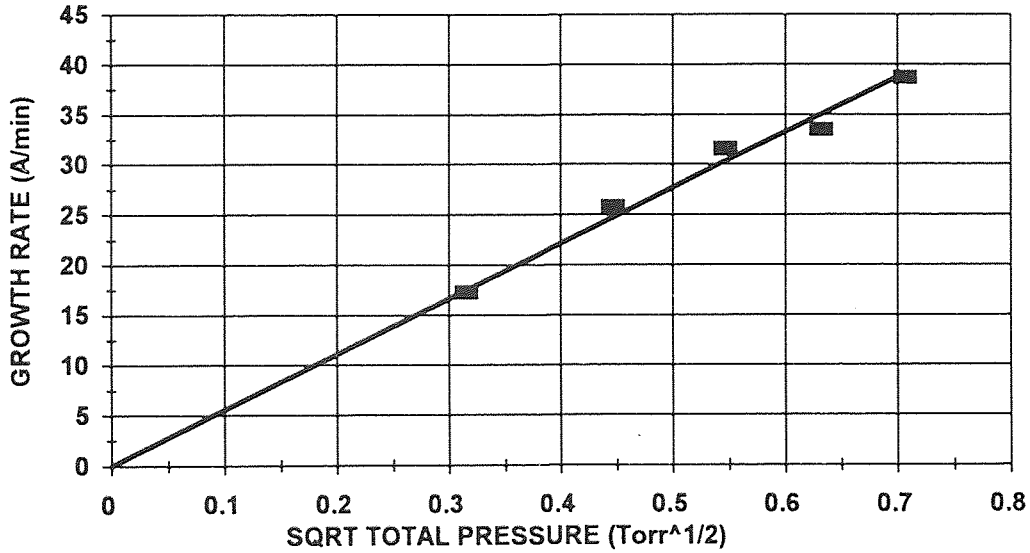

Figure 5.8 Growth Rate as a Function of Square Root of Pressure

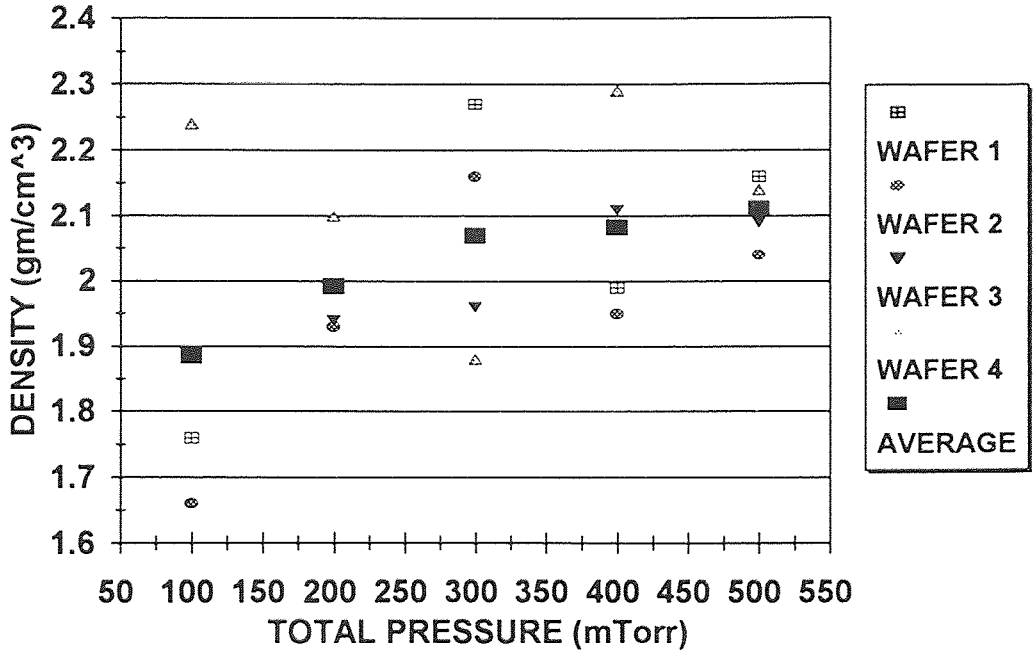

Figure 5.9 Variation of Density of the SiO_2 Deposits with Pressure

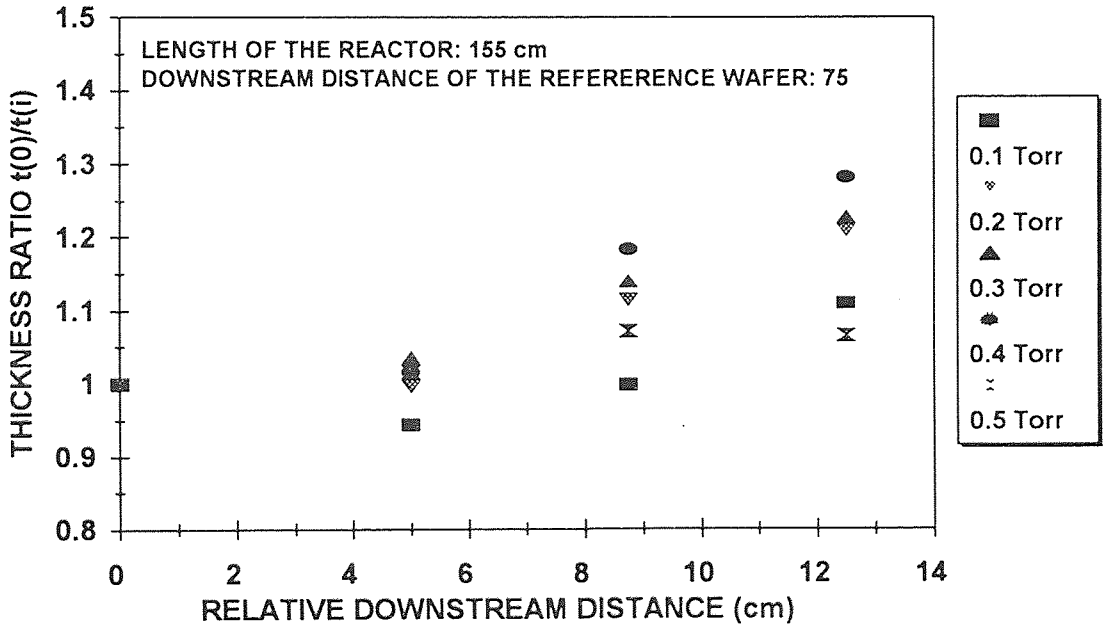

Figure 5.10 Depletion Effects as a Function of Pressure

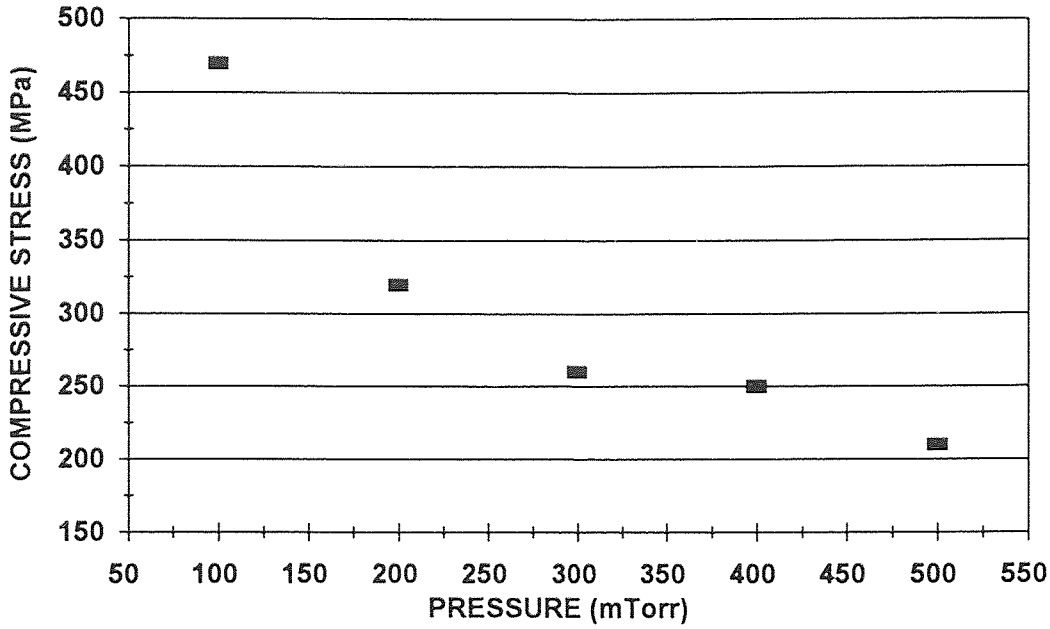

Figure 5.11 Variation of Stress in the Films with Pressure

A general trend from 400 mTorr to 100 mTorr can be observed in Figure 5.10, where depletion along the downstream distance tend to decrease due to increased pumping rate. Although, at 500 mTorr depletion effect is more pronounced than that at 100 mTorr, it is significantly lower than at other pressures studied. This behavior might be attributed to a higher residence time effect which enables saturation of the wafers along the downstream.

Across wafer uniformity in film thickness were within 15 % and the index of refraction was 1.449 ± 0.002 irrespective of the pressure condition. Stress values at all pressures were compressive in nature decreasing with increase in pressure as shown in Figure 5.11.

Density and depletion effects points strongly towards 500 mTorr as being the optimum pressure condition that would provide the optimum oxide plugs for

the mesoporous Vycor support. Within the pressure range investigated, pressure lower than 500 mTorr are therefore not recommended for membrane synthesis.

5.3 Oxygen Flow Rate Series

The oxygen flow rate dependent behavior of deposition rate is shown in Figure 5.12 for constant conditions of temperature (450 °C), total pressure (500 mTorr), and flow rate of DES (30 sccm).

The deposition rate shows a linear dependence with oxygen flow behavior upto 30 sccm as shown in Figure 5.12. This behavior is expected since increasing number of adsorbed oxygen molecules lead to enhanced surface area of the substrate and therefore higher growth in a given time. However, the growth rate started to level off above 30 sccm oxygen flow. This behavior could be attributed to surface saturation and insufficient pumping rates that failed to exhaust the reaction byproducts. When the flow rate was increased beyond 60 sccm (i.e. 90 sccm) ignition of the reactants in the gas phase occurred creating copious amounts of SiO_2 particulates as observed in earlier works (69). No film growth was observed on the wafer surface in good agreement to threshold effects, usually common under conditions of relatively high partial or total pressures. Transition into homogeneous gas phase reaction regime was evidenced by drastic drop in density values with increasing oxygen flow rates as shown in Figure 5.13.

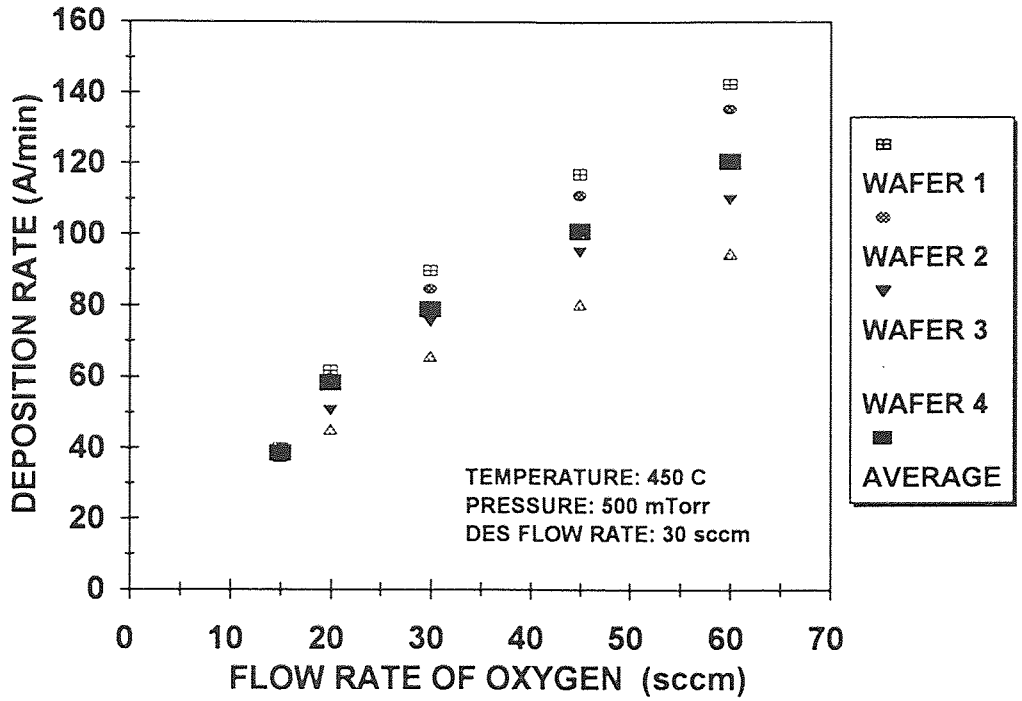

Figure 5.12 Variation of Deposition Rate with Flow Rate of Oxygen

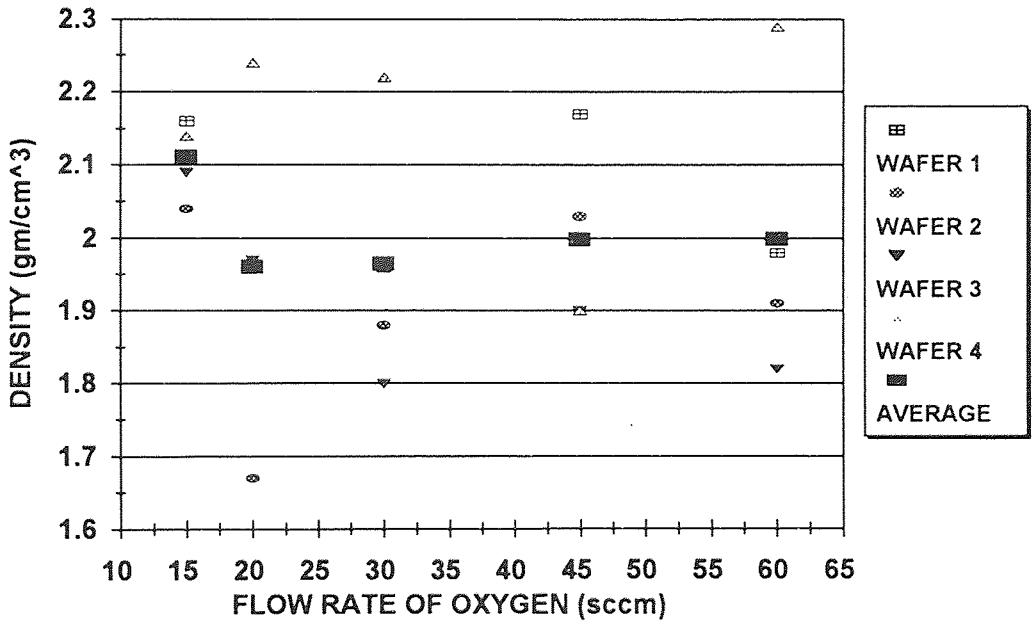

Figure 5.13 Variation of Density of the SiO_2 Deposits with Flow Rate of Oxygen

Moreover, it can be seen from Figure 5.14 that increasing the flow rate of oxygen results in severe downstream depletion effect. Furthermore, from Figure 5.15, it can be seen that stress values suffered a transition from compressive to the tensile nature after flow rate of oxygen was increased to 30 sccm. All these results strongly discourage employing oxygen flow rates higher than 15 sccm.

Irrespective of the reaction conditions the FTIR spectra (Appendix A) showed the presence of peaks due to the stretching and the bending mode at 1052 and 800 cm^{-1}, respectively, of SiO_2 in good agreement with earlier reports (70). Moreover, a peak of small intensity was detected at 880 cm^{-1} and assigned to the H-SiO_3 moiety as observed in previous reports (70).

This effort towards optimization of the variables of a LPCVD process strongly indicated that a temperature of 450 ^0C, a pressure of 500 mTorr and a flow rate of oxygen and DES of 15 and 30 sccm respectively, would yield quality oxides at a moderate growth rate (38.7 Å/min). Oxides deposited employing this set of conditions would be of average density (2.11 g/cm^3), refractive index (1.45), compressive stress (210 MPa), and negligible depletion. Within the range of variables investigated, it is reasonable to apply these reaction conditions for synthesis of SiO_2 on mesoporous Vycor supports.

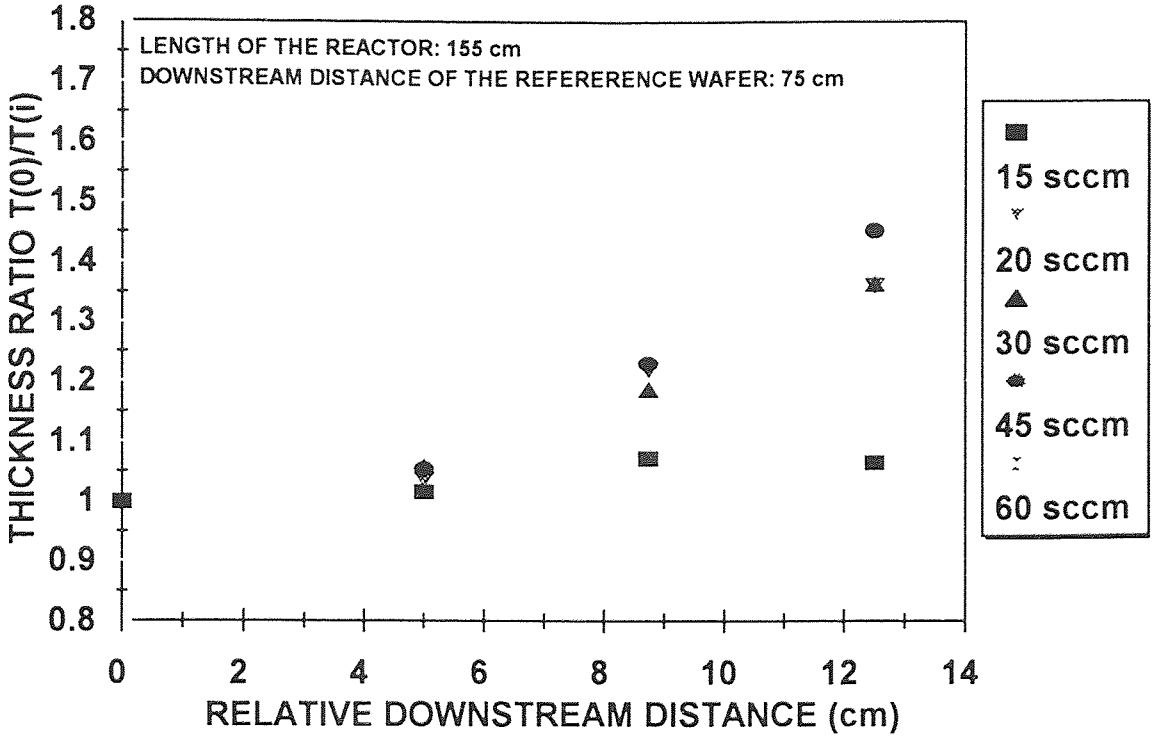

Figure 5.14 Depletion Effects as a Function of Oxygen Flow Rate

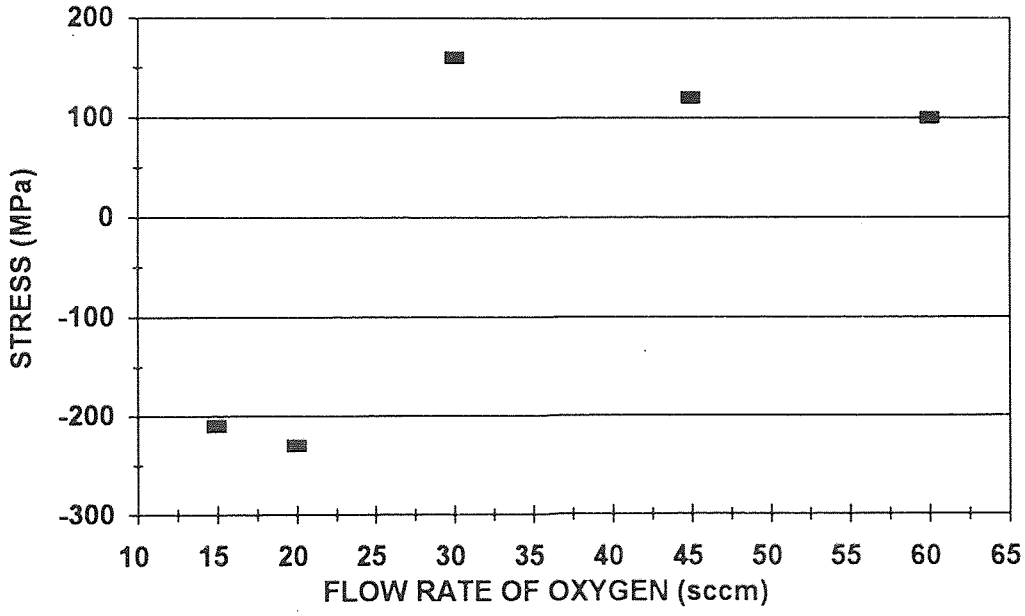

Figure 5.15 Variation of Stress in the Films with Oxygen Flow Rate

5.4 Synthesis of Silicon Oxide/ Vycor Membrane by Same-Side Reaction Geometry

In the same-side reactant geometry procedure 15 sccm oxygen and 30 sccm DES were simultaneously delivered to the chamber side of the LPCVD reactor at a constant pressure of 500 mTorr and temperature 400 ^{0}C. Permeability measurements carried out before deposition, indicated that the flux of the gases were related to the inverse of their molecular weights and exhibited an excellent fit to the Knudsen diffusion curve as shown in Fig. 5.16. Knudsen selectivity across the virgin Vycor also confirmed the absence of microcracks and defects in the mesoporous structure. Such a confirmation is of extreme importance because defects such as pinholes in the substrate structure might fill up during deposition resulting in a sudden drop in permeability. This would, in turn, lead to erroneous evaluation of membrane performance. In-situ permeabillity measurements was carried out after a initial deposition time of 2 hr.

From Figure 5.16 it could be observed, that permeability values for all the gases decreased significantly indicating the formation of deposits on the porous Vycor support. However, the extent of decrease of permeability across the membrane is not the same for all gases and therefore all of them cannot be fitted onto a Knudsen type of behavior under these conditions. Knudsen diffusion theory is independent of the size of the permeates, and therefore any deviation from it would suggest a flux regime where size effects become important. It is also evident from Fig. 5.16, that He experiences the least resistance to transit across the composite membrane.

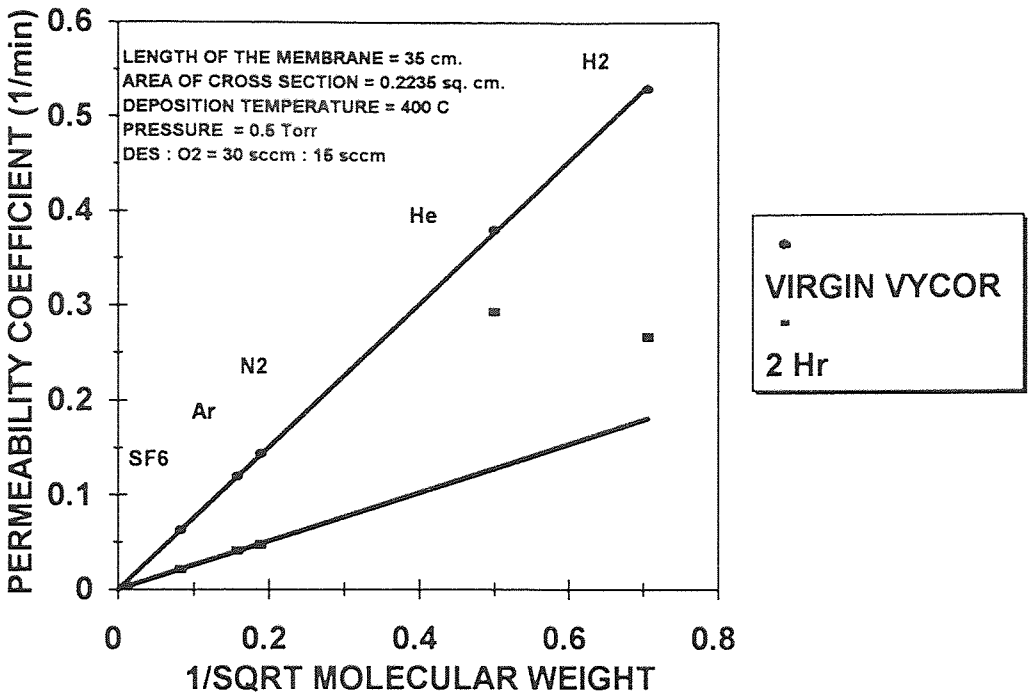

Figure 5.16 Permeability Coefficients across Silicon Oxide/ Vycor Membrane for the Same Side Geometry

In fact, taking the virgin Vycor substrate as the reference, decrease in H_2 permeability (45.6 %) is significantly higher than the drop in He permeability (23.6 %). This phenomena could be explained by considering the fact that He (Van-der Waals diameter 2.55 Å) is a smaller molecule than H_2 (Van-der Waals diameter 2.83 Å) and therefore it can permeate faster through the tortuous pore channels at an equivalent pressure differential. Permeates such as, N_2, Ar and SF_6 however, exhibit equal drops (6.6 %) in permeability and thus their permeation characteristics are still governed by the mass effects as predicted by Knudsen. As discussed earlier in the thesis, the ratio of the permeability coefficients for gases governed by size as opposed to those governed by mass would yield a value higher than Knudsen selectivity. After two hours of

deposition size selectivity of He/N_2 and H_2/N_2 were 6 and 5.5 respectively, higher than that of the Vycor support. Selectivity beyond Knudsen, however, was not observed for N_2/SF_6.

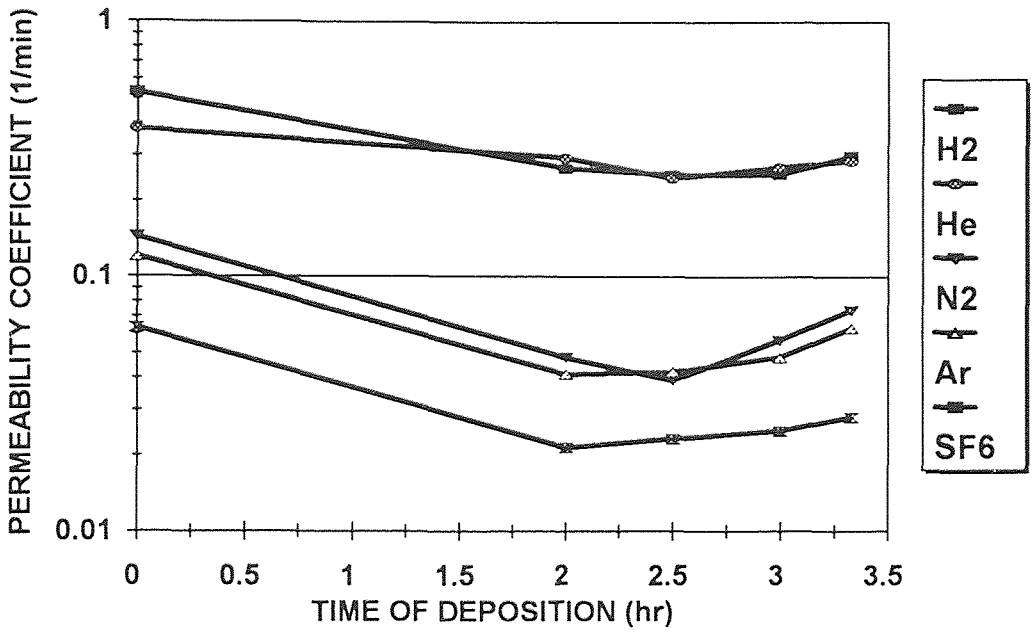

Figure 5.17 Permeability Coefficient as a Function of Deposition Time for Same Side Geometry

After subsequent depositions, variations in permeability showed an interesting behavior when permeability coefficient (on a log scale) was plotted against time of deposition (on a linear scale) in Figure 5.17. Irrespective of the permeate, flux across the SiO_2/ Vycor membrane leveled off and then began to increase in spite of increase in deposition time. This unexpected behavior indicates the onset and development of cracks, which were visible under the optical microscope, with increasing oxide film thickness. The deposition conditions used for membrane fabrication is within the bounds of

surface reaction rate limited regime as confirmed by our previous study on silicon wafers. However, flat surface geometries of Si wafers are quite different from complex surface contours present in the mesoporous Vycor support. Although, average pore size in the Vycor substrate is reported in literature to be of much larger than atomic dimensions (i.e., 40 Å), the probability of pore channels narrowing down into much reduced dimensions is high. Depending on membrane tortuosity, resistance to diffusion of the reactants through the pore channels will vary leading to a wide distribution of deposition profiles (18). Moreover, reactants approaching the Vycor from the same side will have a higher chance for reacting on the surface of the support tube under the low flux conditions in the pore channels. This effect will be more pronounced with increasing deposition time as blockage of pore plugs creates pore wall effects increasing the activation energy for diffusion (39). Such a surface-dominant deposition profile have been revealed under SEM investigations and reported in literature (32). Increasing surface deposition will result in increasing film thickness eventually leading to the loss of film integrity as seen in our study. Nevertheless, this work has been successful in fabricating a SiO_2/ Vycor composite membrane employing an LPCVD process. Earlier attempts towards such an endeavor did not yield positive results (30). Moreover, the results strongly suggested that the efficacy of microengineering pore structure for selectivity at appreciable permeation rates resides on achieving more reactions, at a controlled rate, inside the pore channels rather than at the surface. With this aim, a counter-diffusion reactant geometry was then investigated.

5.5 Synthesis of Silicon Oxide/ Vycor Membrane by Opposing Reaction Geometry

Oxygen and DES streams were introduced at opposite sides of the tubular Vycor support. Flow rates of oxygen was adjusted to achieve a steady pressure of 4 Torr inside the Vycor tube, while DES vapor was pumped in the reaction chamber concentric to the membrane module and kept stagnant at a pressure of 8 Torr.

Permeability measurements after 3 hr deposition indicated similar behavior to that observed for the same side reaction geometry, as shown in Figure 5.18. Immediate effects of high selectivity of the silica membrane towards H_2 permeation consistent with literature was observed (72). Moreover, the flux for He across the membrane showed a very slight decrease after 3 hr deposition in good agreement with previous work (67, 73).

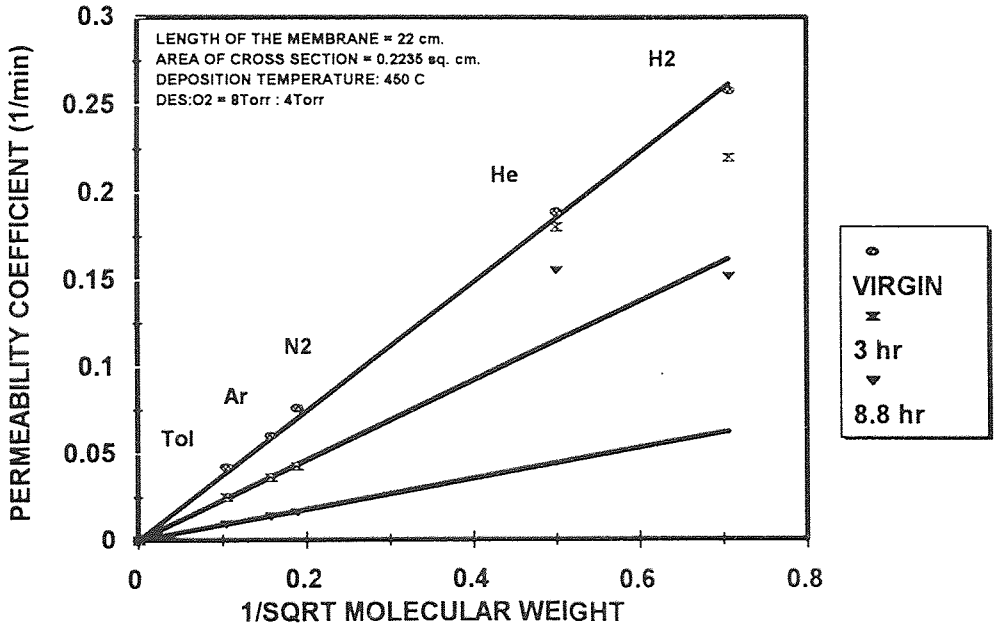

Figure 5.18 Permeation Across the Silicon Oxide/ Vycor Composite Membrane for Opposing Geometry

The slope of the Knudsen curve In Figure 5.18 (permeability coefficient * square root MW) was plotted as a function of the kinetic diameter of the permeates in Figure 5.19. That Knudsen diffusion is independent of molecular size is clearly evident from such a plot for the Vycor tube. After 3 hr SiO_2 deposition, however, onset of size effects on flux across the membrane is visible from Figure 5.19, between He, H_2, and N_2, Ar, and toluene and is indicative of selectivity values higher than those predicted by Knudsen. However, beyond-Knudsen selectivity was not observed between N_2, Ar and toluene. Initiation of size selectivity also implied transition from the mesoporous structure present in the virgin Vycor substrate to a microporous regime probably due to a pore filling effect (32).

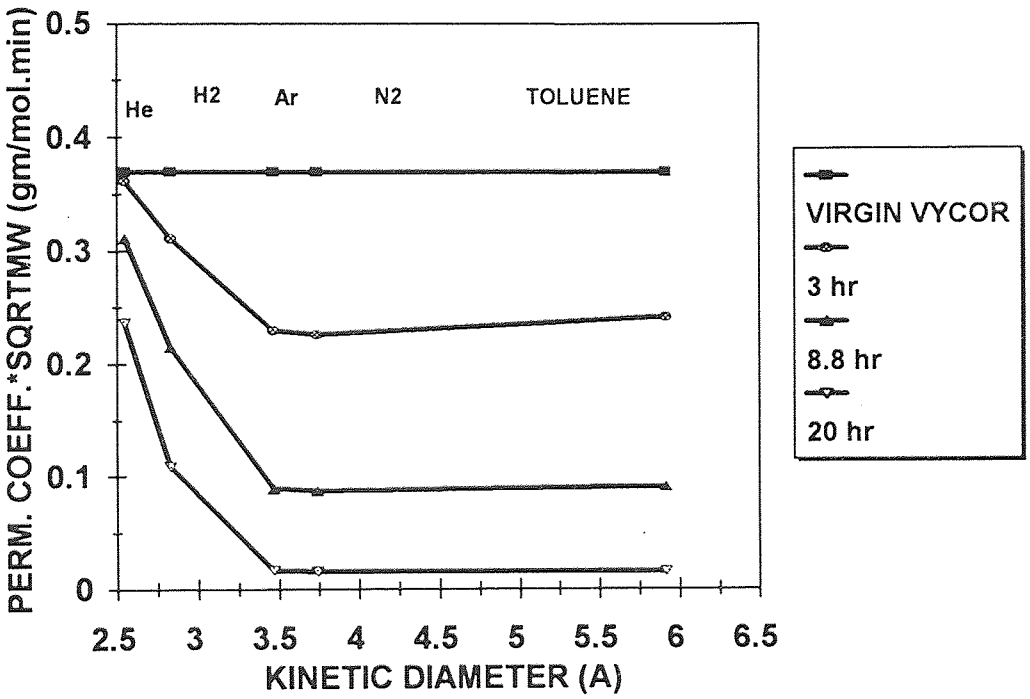

Figure 5.19 Deviation from Knudsen Behavior with Deposition Time

To have a better insight into the pore plugging process, permeability coefficients, of the set of permeates, were plotted as function of deposition time on a semilog scale (see Figure 5.20). Contrary to the same side reaction geometry process, no signs of cracking were observed even after long periods of deposition. This is evidenced by the monotonic decrease of flux across the membrane with deposition time for all permeates. Furthermore, this behavior strongly indicated that a shift of the reaction site from the surface of the support to the insides of the pore channels had occurred, justifying the efficacy of the opposing reaction geometry technique (30).

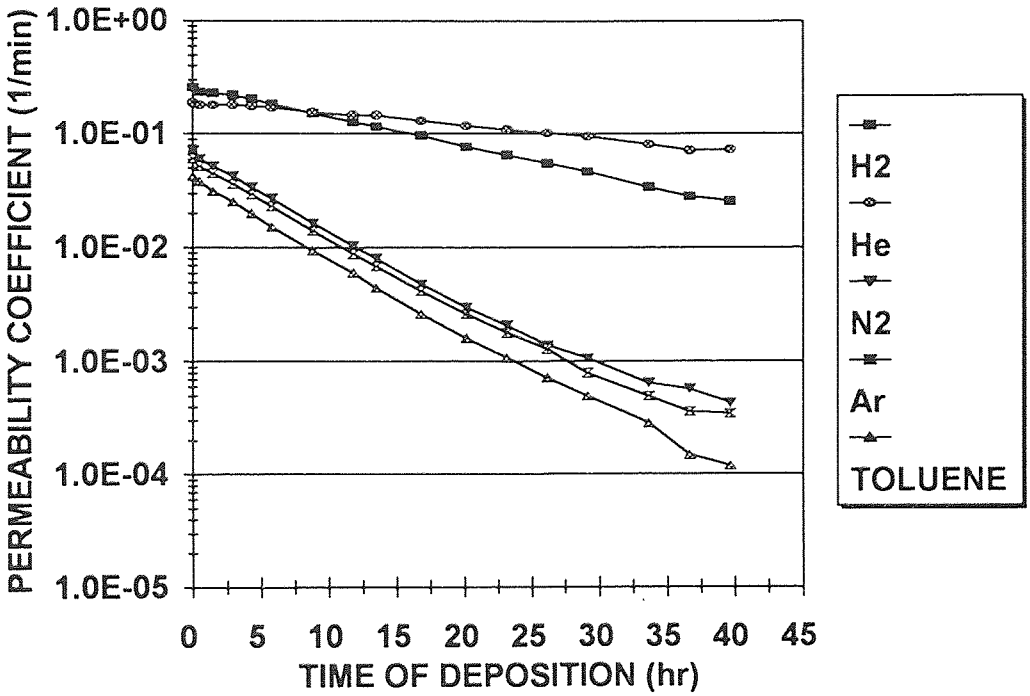

Figure 5.20 Decrease in Permeability Coefficient as A Function of Deposition Time

Moreover, this observation is in excellent agreement with previous attempts to synthesize membranes using this approach (30-31, 73). The success of the opposing geometry technique over the same side geometry approach can possibly be understood by considering that counterdiffusing reactant streams, driven by a pressure and/or a concentration gradient, have higher probability of meeting and reacting in a narrow front within the tortuous pore channels than at the substrate surface.

Furthermore, the time evolution plot of the pore-plugging process in Figure 5.20 revealed two interesting observations. After approximately 8 hr deposition time a crossover point similar to that reported by Nam et al. (73), was seen when H_2 permeability decreased below He. They also observed and reported that, He and H_2 show activated diffusion mechanisms, and therefore, their permeation characteristics seemed to be strongly influenced by wall effects (39, 67). This behavior strongly emphasized a transition from the mesoporous Vycor into a microporous regime where diffusing molecules migrated against the potential barrier exerted by the micropore walls. Under, these circumstances, simpler and monoatomic molecules like He would diffuse much more easily when compared to the other permeates, as evidenced by the smaller decrease in its permeability coefficient values with deposition time (see Figure 5.20).

The second important observation from Figure 5.20 is the lack of size selectivity between N_2 and toluene until about 34 hr deposition. Moreover, a sharp drop in N_2 permeability, as reported in literature (73), around the H_2-He crossover point was not observed in our study. However, in the above-mentioned work it was reported that, the silicon oxide/ Vycor membrane was

annealed after periods of deposition which resulted in a densification of the deposits. Thus, a drastic decrease in N_2 permeability, was not observed across our membrane structure due to the presence of pinholes in our oxide plugs which allowed Knudsen diffusion of N_2, Ar, and toluene. This phenomena of leakage of N_2 had also been observed by Kitao et al. (67). The presence of pinholes, on the other hand, could be due to a combination of the low density of the deposits and depletion effects (as evidenced by the wafer deposition study). Non-uniform or broad pore size distribution in the vycor substrate could possibly be an added factor since the larger pores would allow Knudsen diffusion even when the smaller pores were be completely plugged by the oxide,

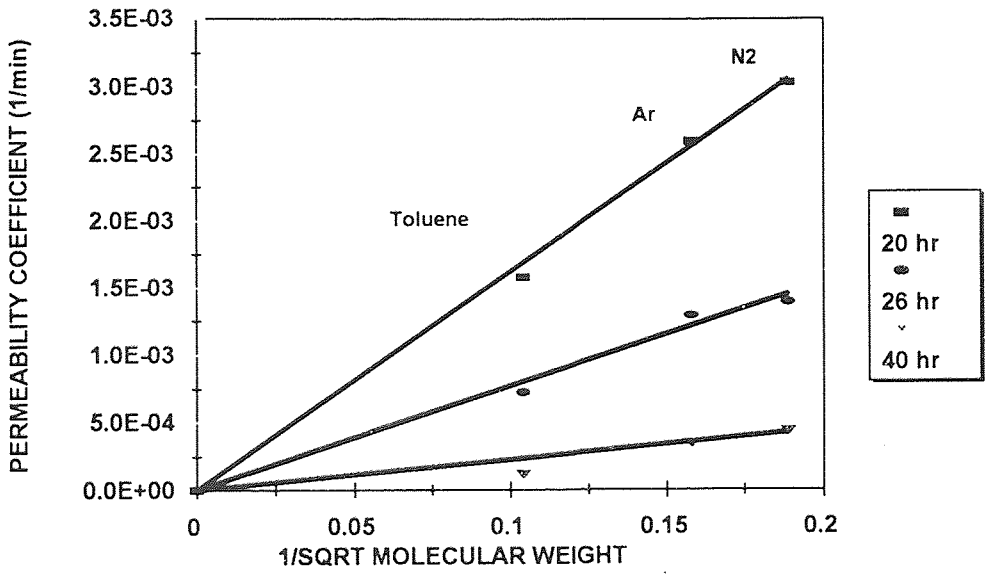

Figure 5.21 Permeation Across Silicon Oxide/ Vycor Composite Membrane after 20 hr Deposition

After about 26 hr of deposition, the diffusion of toluene deviated from the Knudsen mode as seen in Figures 5.21 and 5.22. However, selectivity between nitrogen and toluene were achieved at very low permeability coefficient values

consistent with our understanding that the process of plugging the pin-holes in the oxide had led to further undesired clogging of pores already selective to N_2 permeation.

The selectivity values calculated as ratios of permeability coefficient were plotted as a function of deposition time in Figures 5.23-5.25. After 40 hr deposition the selectivity values were He/N_2 = 169, He/toluene = 613, H_2/N_2 = 59, H_2/toluene = 214, and N_2/toluene = 3.63. However, the growth rate of the deposits were very slow probably due to the stagnant condition maintained inside the CVD reaction chamber, which might have had affected the equilibrium reaction rates unfavorably. Since reaction by-products were not exhausted, they might had been instrumental in producing porous oxide deposits.

Nevertheless, slow growth rates was ideal for the studying the trends in permselectivity variation. The selectivity values for He and H_2 with respect to N_2 are in close agreement to those reported in literature (32). Furthermore, there was novel indications of N_2/toluene selectivity beyond Knudsen. Therefore, it could be concluded that a low pressure vapor deposition process can be effectively employed to tailor-make silicon oxide/Vycor composite membranes for high temperature gas separation processes, for catalytic membrane reactor applications and even in environment clean-up operations as VOC barriers.

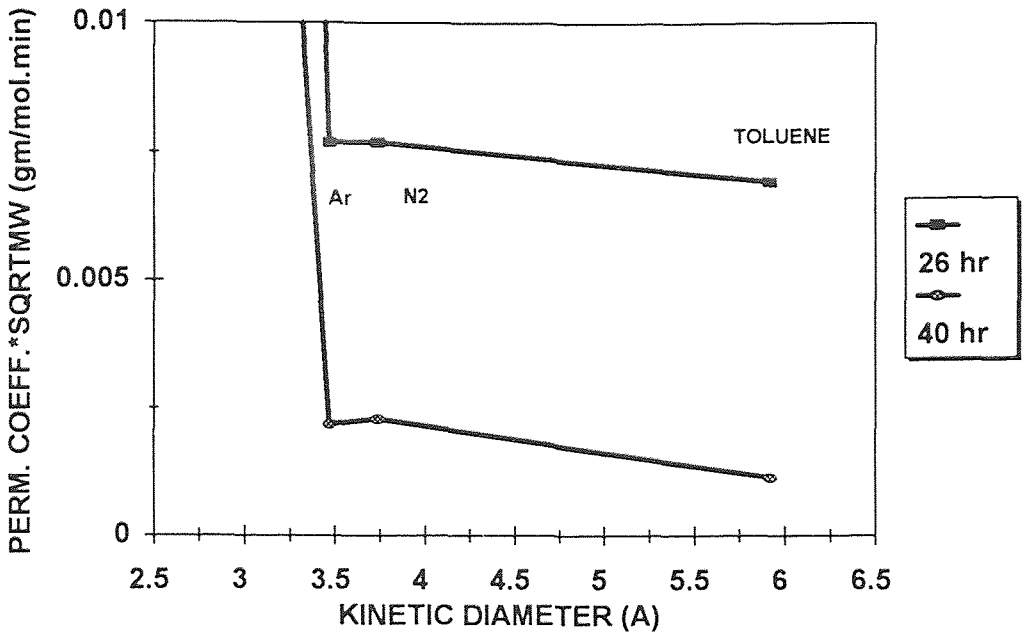

Figure 5.22 Deviation from Knudsen behavior after 26 hr Deposition

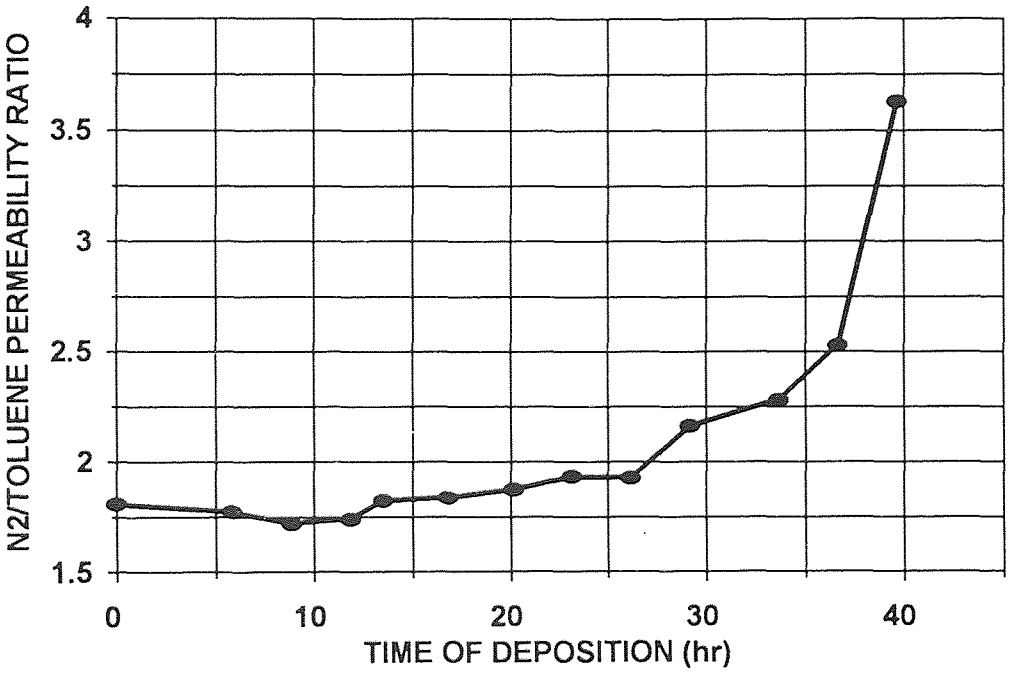

Figure 5.23 Nitrogen/ Toluene Permeability Ratio as a Function of Deposition Time

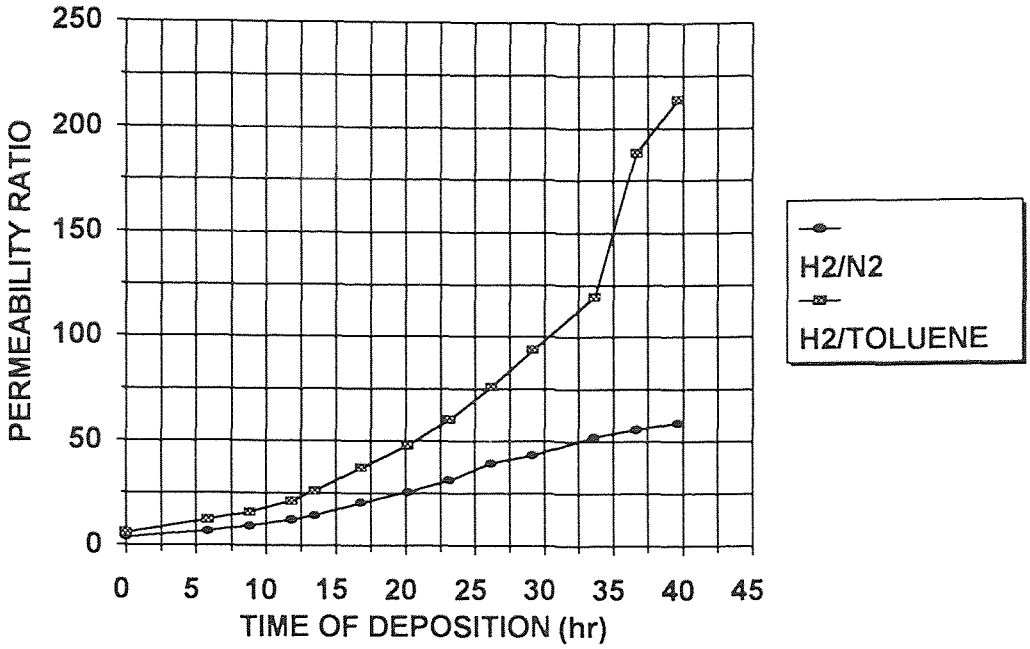

Figure 5.24 Permeability Ratios of Hydrogen to Nitrogen and Toluene

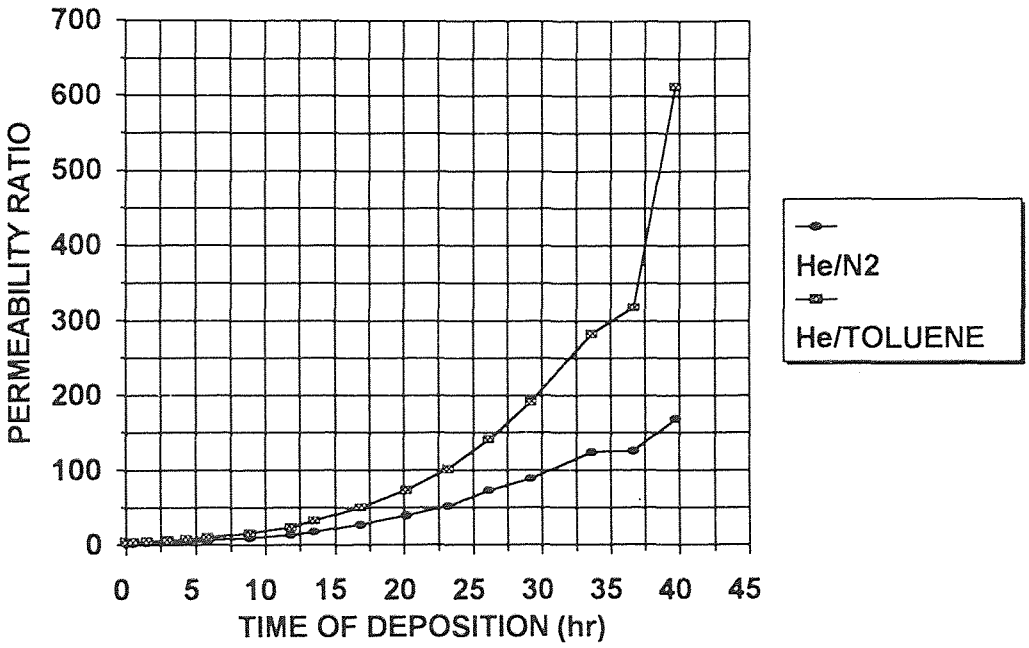

Figure 5.25 Permeability Ratios of Helium to Nitrogen and Toluene

CONCLUSION

Diethylsilane was used as a precursor to synthesize silicon oxide films on <100> wafers and later on tubular Vycor tubes employing a low pressure chemical vapor deposition process. Film deposition on silicon wafers was undertaken with the aim to optimize the variables of the LPCVD process in order to obtain a suitable deposition condition that would yield a suitable oxide for subsequent membrane synthesis. Growth rates were studied as a function of process parameters such as, temperature, total pressure and flow rate of oxygen. The results indicated that at a temperature of 450 ^{0}C, total pressure of 500 mTorr and oxygen and DES flow rates of 15 sccm and 30 sccm would yield a suitable silicon oxide deposit with density = 2.11 g/cm^3, RI = 1.45, and compressive stress = 210 MPa. Moreover, the growth rate was found to show an Arrhenius dependence with temperature over the range 375 ^{0}C - 475 ^{0}C. IR spectra indicated the presence of hydrogen bonded silanol groups Si-OH at 880 cm^{-1} in addition to the Si-O streching and bending peaks at 1052 cm^{-1} and 800 cm^{-1} respectively. A reaction condition of 500 mTorr, 15 sccm and 30 sccm flow rates of oxygen and DES respectively and 400 ^{0}C was used to deposit oxide films on tubular Vycor supports which was closed at one end. The reactant streams were fed on the same (chamber) side of the support. The same-side deposition geometry approach was successful in achieving significant deposition on the Vycor support as reflected by decreases in permeability of the gases. Progressive deposition led to increase in permeabilty for all gases across the membrane, indicating deposition on the surface of the Vycor substrate followed by cracking of the membrane structure. The opposing reactant geometry

technique was then attempted and good selectivity values, which are in agreement with those reproted in literature, were observed.

APPENDIX A

FTIR Spectra

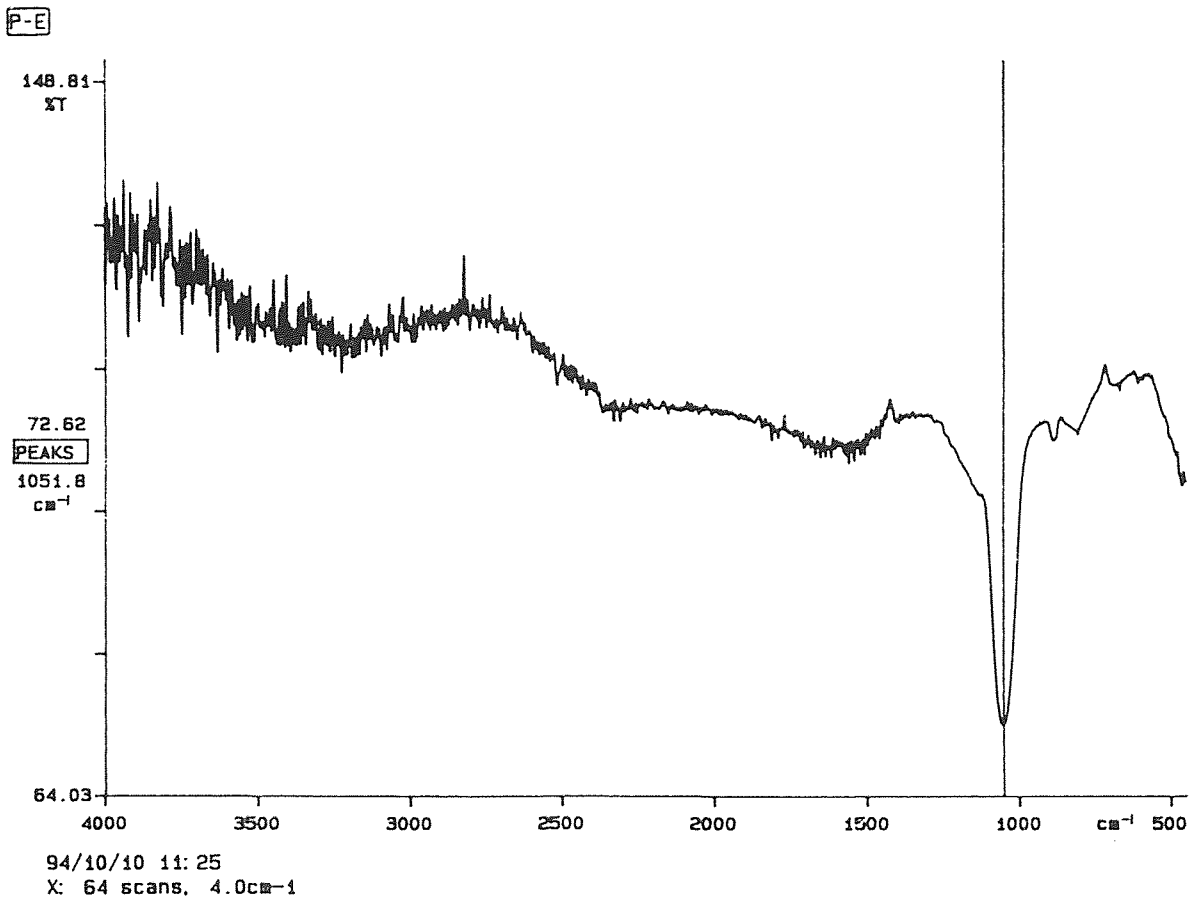

FIGURE A.1 FTIR Spectra of the Films Deposited on Silicon Wafers

REFERENCES

1. Teramoto, M.H., Matsuyama, T., Yamashiro, S. and Okamoto, P. Separation of ethylene from ethane by flowing liquid membrane using silver nitrate as a carrier. *J. Membane Sci.* 1992, **45**, 593

2. Guha, A.K., Majumdar, S., and Sirkar, K.K. Gas separation modes in a hollow fiber contained liquid membrane permeator. *Ind. Eng. Chem. Res.* 1992, **31**, 593

3. Xu, Q., and Anderson, M.A. Synthesis of porosity controlled ceramic membranes. *J. Mater. Res.* 1991, **6(5)**, 1073

4. Lin, Y.S., de Vries, K.J., Burggraaf, A.J., and de Haart, L.G. A kinetic study of the electrochemical vapor deposition of solid electrolytic films on porous substrates. *J. Proc. Electrochem. Soc.* 1990, **137**, 3960

5. Palmer, J.R., and Kaczenski, M.E. *Economics Benefits from Alternate Applications of DOE Inorganic Membrane Technology*. November, 1992.

6. Sing, K.S.W., Everret, D.H., Haul, R.A.W., Moscou, L., Pierotti, L.R.A., Rouquerol, J., and Siemieniewska, T. Physiosorption data for gas/ solid systems with special reference to the determination of surface area and porosity. *Pure and Appl. Chem.* 1985, **57**, 603

7. Hsieh, H.P. Inorganic membranes. *AICHE Symp. Ser.* 1988, **84**, 261

8. Gryzanov, V.M. Hydrogen permeable paladium membrane catalyst. *Platinum Met. Rev.* 1986, **30**, 68

9. Edlund, D.J., and Pledger, W.A. Thermolysis of hydrogen sulphide in a metal-membrane reactor. *J. Membrane. Sci.* 1993, **77**, 255

10. Hsu, C.Z., and Buxbaum, R.E. Palladium catalyzed oxidative diffusion for tritium extraction. *J. Nuc. Met.* 1986, **141**, 238

11. Collins, J.P., and Douglas, W. Preparation and characterization of a composite palladium-ceramic membrane. *Ind. Eng. Chem. Res.* 1993, **32**, 3006

12. Uemiya, S., Sato, N., Ando, H., Kude, Y., Sugino, K., Matsuda, T., and Kikuchi, E. Separation of hydrogen through palladium thin film supported on a porous glass tube. *J. Membrane Sci.* 1991A, **56**, 303

13. Koresh, J.E., and Sofer, A. The carbon molecular sieve membranes. General properties and the permeability of CH_4/H_2 mixture. *Separation Sci. Technol.* 1987, **22**, 973

14. Hsieh, H.P. General characteristics of inorganic membranes. in: Bhave, R.R. Ed., *Inorganic Membranes: Synthesis, Characteristics and Applications,* Van Nostrand Reinhold, New York, 1991

15. Lee, L.H., and Hwang, S.T. A new silicon-based material formed by pyrolysis of silicon rubber and its properties. *Chem. Eng. Commun.* 1986, **44**, 121

16. Shelekhin, A.B., Dixon, A.G., and Ma, Y.H. Adsorption, diffusion and permeation of gases in microporous membranes, part I. *J. Membrane Sci.* 1991, **75**, 221

17. Shelekhin, A.B., Dixon, A.G., and Ma, Y.H. Adsorption, diffusion and permeation of gases in microporous membranes, part II. *J. Membrane Sci.* 1992, **75**, 233

18. Shelekhin, A.B., Dixon, A.G., and Ma, Y.H. Adsorption, diffusion and permeation of gases in microporous membranes, part III. *J. Membrane Sci.* 1993, **83**, 181

19. Tomadakis, M.M., and Sotirchos, S.V. Effective Knudsen diffusivities in structures of randomly overlapping fibers. *AIChE J.* 1991, **37**, 74

20. Yoldas, B. E. Alumina sol preparation from alkoxides. *Ceram. Bulletin.* 1975, 54, 289

21. Gieselmann, M.J., Anderson, M.A., Moosemiller, M., and Hill, D. Physicochemical properties of supported and unsupported γ-Al_2O_3 and TiO_2 ceramic membranes *Sep. Sci. Technol.* 1988, **23**, 1695

22. Leenaars, A.F.M., Keizer, K., Burggraaf, A.J. The preparation and characterization of alumina membranes with ultrafine pores, part I. Microstructural investigations of nonsupported membranes. *J. Mater. Sci.* 1984, **19**, 1077

23. Larbot, A., Alary, J.A., Guizzard, C., Cot, L., and Gillot, J. New inorganic ultrafiltration membranes: titania and zirconia membranes. *J. Am. Ceram. Soc.* 1989, **72**, 257

24. Larbot, A., Alary, J.A., Guizzard, C., Cot, L., and Gillot, J. Silica membranes by the sol-gel process. *J. Membrane Sci.* 1989, **44**, 289

25. Uhlhorn, R.J.R., Keizer, K., and Burggraaf, A.J. Gas and surface diffusion in modified γ-alumina systems. *J. Membrane Sci.* 1989, **46**, 225

26. Uhlhorn, R.J.R., Huis, M., Keizer, K., and Burggraaf, A.J. Gas transport and separation with ceramic membranes, part II. synthesis and separation properties of microporous membranes. *J. Membrane Sci.* 1992, **66**, 271

27. Hammel, J.J. Porous inorganic siliceous-containing gas enriching material. *U. S. Patent.* 4,853,001,.August 1, 1989

28. Hammel, J.J. Direct measurement of homogeneous nucleation rates in a glass-forming system. *J. Chem. Phys.* 1967, **46**, 2234.

29. Furneaux, R.C., Rigby, W.R., and Davidson, A.B. The formation of controlled-porosity membranes from anodically oxidized aluminum. *Nature.* 1989, **337**, 147

30. Gavalas, G.R., Megiris, C.E., and Nam, S.W. Deposition of H_2-permselective SiO_2 films. *Chem. Eng. Sci.* 1989, **44**, 1829

31. Gavalas, G.R., and Megiris, C.E. Synthesis of SiO_2 membrane on porous support and method of use of same. *U. S. Patent.* 4,902,307, 1990

32. Megiris, C.E., and Glezer, J.H.E. Synthesis of H_2-permselective membranes by modified chemical vapor deposition. Microstructure and permselectivity of SiO_2/C/Vycor membranes. *Ind. Eng. Chem. Res.* 1992, **31**, 1293

33. Okubu, T., and Inoue, H. Introduction of specific gas selectivity to porous glass membranes by treatment with tetraethoxysilanes. *J. Membr. Sci.* 1989, **42**, 109

34. Okubu, T., and Inoue, H. Single gas permeabilities through porous glass modified with tetraethoxysilane. *AICHE J.* 1989, **35(5)**, 845

35. Gupte, S.M., and Tsamopolous, J.A. An effective medium approach for modeling chemical vapor Infiltration of porous materials. *J. Electrochem. Soc.* 1990, **137(5)**, 1626

36. Barrer, R.M. *Zeolites and Clay Minerals as Sorbents and Molecular Sieves.* Academic Press, New York, 1978

37. Breck, D.W. *Zeolite Molecular Sieves.* Krieger, R.E. Publishing Company, Florida, 1984

38. Te Hennepe, H.J.C., Bargeman, D., Mulder, M.H.V., and Smolders, C.A. Zeolite-film silicon rubber membranes, part I. Membrane preparation and pervaporation results. *J. Membrane Sci* 1987, **35**, 39

39. Way, J.D., and Roberts, D.L. Hollow fiber inorganic membranes for gas separation. *Sep. Sci. Technol.* 1992, **27**, 29

40. Hwang, S.T., and Kammermeyer, K. *Membranes in Separations*. Krieger, R. E. Publishing Company, Florida, 1984

41. Present, R.D. *Kinetic Theory of Gases*, McGraw-Hill, New York, 1958

42. Fain, D.E. Membranes gas separation principles. *MRS Bulletin.* 1994, April, 40

43. Yang, R.T. *Gas Separation by Adsorption Processes*. Butterworths, Boston, Massachusetts, 1987

44. Lee, K.H., and Hwang, S.T. The transport of condensible vapors through a microporous vycor glas membrane. *J. Colloid Interface Sci.* 1986, **110**, 545

45. Asadea, M., and Du, L.D. Separation of alcohol/water gaseous mixtures by thin ceramic membranes. *J. Chem. Engr. Japan.* 1986, **19**, 72

46. Kapoor, A., Yang, R.T., and Wong, C. Surface diffusion. *Catal. Rev. Sci. Eng.* 1989, **31**, 129

47. Van Vuren, R.J., Keizer, K., and Burgaraaf, A.J. Gas separations with modified ceramic alumina membranes, Paper 9-P02, *International Congress on Membranes*. Tokyo, Japan. June 8, 1987

48. Smith, D.M., Hua, D.W., and Earl, L.W. Characterization of porous solids *MRS Bulletin*. 1994, April, 44

49. Cuperus, F.P., Bargeman, D., and Smolders, C.A. Permporometry: the determination of size distribution of active pores in ultrafiltration membranes. *J. Membrane Sci.* 1992, **71**, 57

50. Cao, G., Brinkman, H.W., Meijerink, J., de Vries, K.J., and Burggaraaf, A.J. Pore narrowing and formation of ultrathin yttria-stabilized zirconia by chemical vapor deposition/electrochemical vapor deposition. *J. Am. Ceram. Soc.* 1993, **76**, 2201

51. Mey-Marom, A., and Katz, M. Measurement of active pore size distribution of microporous membranes: A new approach. *J. Membrane. Sci.* 1986, **27**, 119

52. Derome, A.E. *Modern NMR Techniques for Chemistry Research*. Pergamon Press, Oxford, 1987

53. Van den Berkel, C.H.J. *Chemical Vapor Deposition*. Blocher, J.M., Vuilland, G.E., and Wahl G. Eds., The Electrochemical Society, Pennigton, New Jersey, U. S. A., 1986

54. Kern, W. Chemical vapor deposition. Levy, R.A. Eds., *Microelectronic Materials and Processes*. Kluwar Academic, New Jersey, U. S. A., 1986

55. Middlemann, S., and Yeckel., A. The origin of non-uniform growth of LPCVD films from silane gas mixture. *J. Electrochem. Soc.* 1989, **137(7)**, 2038

56. O'Mara, W.C., Herring, R.B., and Hunt, L.P. *Handbook of Semiconductor Silicon Technology*. Noyes Publications, New Jersey, U.S.A., 1990

57. Weiss, A. PECVD: silicon nitride and beyond. *Semiconductor International*. 1983, **6(7)**, 88

58. Tanikawa, E., Okabe, T., and Maeda, K. *Doped Oxide Films by Chemical Vapor Deposition*. Wakefield, G.F., and Blocher J.M. Eds., The Electrochemical Soc. Princeton, New Jersey, U.S.A., 1973

59. Coulson, A.R., and Tauber, R.N. Silicon processing for the VLSI era. *Solid State Technol.* 1979, **63**, 61

60. Hammond, M. Introduction to chemical vapor deposition *Solid State Technol.* 1979, **63**, 74

61. Cobianu, T., and Pavelescu, C. Silane oxidation in LPCVD systems in the tempearture range 100-450 ^{0}C. *Thin Solid Films.* 1984, **117**, 211

62. Pilskin, W.A., Kerr, D.R., and Perri, J.A. *Physics of Thin Flims.* Hass, G., and Then, R.E. Eds., Academic, New York, 1967

63. Pilskin, W.A. Comparison of properties of dielectric films deposited by various methods. *J. Vac. Sci. Technol.* 1977, **14**, 1064

64. Schnabel, R., and Vaulont, W. High pressure techniques with porous glass membranes. *Desalination.* 1978, **24**, 249

65. Blocher, J.M. Coating of glass by chemical vapor deposition. *Thin Solid Films*. 1981, **77**, 51

66. Lee, R.W. Diffusion of hydrogen in natural and synthetic fused quartz. *J. Chem. Phys.* 1963, **38**, 448

67. Kitao, S., and Asadea, M. Gas separation performance of thin porous silica membrane prepared by sol-gel and CVD methods. *Key Eng. Mater.* 1991, **61** & **62**, 267

68. Boyd, D.C., and Thompson, D.A. Glass. *Encyclopedia of Chemical Technology.*1980, **11**, 807.

69. Patterson, J.D., and Ozturk, M.C. Low pressure chemical vapor deposition of silicon dioxide below 500 ^{o}C by the pyrolysis of diethylsilane in oxygen. *J. Vac. Sci. Technol. B.* 1992, **10(2)**, 625

70. Levy, R.A., Grow, J.M., and Chakravarthy, G.S. Low-pressure chemical vapor deposition of silicon dioxide using diethylsilane. *Chem. Mater.* 1993 **5(12)**, 1710

71. Atkins, P.W. *Physical Chemistry.* Freeman W.H. and Company, San Francisco, U.S.A., 1992

72. Altemose, V.O. Helium diffusion through glass. *J. Appl. Phys.* 1961, **32**, 1309

73. Nam, S.W., and Gavalas, G.R. Stability of H_2-permselective SiO_2 films formed by chemical vapor deposition. *AIChE Symp. Ser.* 1990, **85**, 68